



## Principal component analysis of biological and physical variability in a Gulf Stream meander crest

ARTHUR J. MARIANO,\* GARY L. HITCHCOCK,\*  
CARIN J. ASHJIAN,\*† DONALD B. OLSON,\* TOM ROSSBY,‡  
EDWARD RYAN\* and SHARON L. SMITH\*

(Received 27 October 1994; in revised form 23 August 1995; accepted 10 October 1995)

**Abstract**—In September and October 1988 a series of physical and biological observations were collected by the R.V. *Endeavor* and R.V. *Cape Hatteras* in a Gulf Stream meander crest. The hydrographic data, vertical chlorophyll *a* profiles derived from CTD/fluorescence profiles (calibrated with discrete pigment samples), and zooplankton biomass data (20–120 m, estimated from MOCNESS calibrated ADCP profiles) are here analyzed by means of a Principal Component Analysis (PCA). The PCA of salinity, temperature, density, chlorophyll *a*, and zooplankton biomass are performed relative to the cross-sectional average of each. The cross-sectional averages explain 80%, 80%, 54%, 50%, and 18% of the variability for density, temperature, salinity, chlorophyll *a* and zooplankton biomass, respectively. The first two vertical statistical modes for both temperature and density explain almost 90% of the remaining variability relative to the corresponding cross-sectional average, and those for salinity explain more than 80% of the detrended variability. The first two chlorophyll and zooplankton modes explain relatively less of the detrended variability: 60% and 70%, respectively. The first vertical modes of all the physical variables are relatively coherent in the upper 100 m, while that of chlorophyll *a* exhibited increased variability in the upper 120 m with a zero-crossing at 55 m. The first mode of zooplankton biomass is near-surface intensified and decreases between 40 and 100 m.

For each variable, the individual profiles are regressed onto the corresponding modes to generate a spatial/temporal series of the first two principal components. These series are analyzed in a local curvilinear coordinate system, defined by the apex of the meander crest on a daily basis. The spatial structures of the principal components for each of the physical variables in the curvilinear coordinate system are very similar. The temporal variability in this data set is overwhelmed by the spatial variability for all variables except zooplankton biomass, which exhibits a clear diurnal signal because of diel migration. For all the variables, cross-stream variability dominates, but there is some indication of along-stream variability, particularly in the Slope Water. The large-scale Gulf Stream front produces 50–80% of the total data variance in all variables, except the zooplankton. Mesoscale phenomena, including meander-induced vertical motion with associated detrainment/entrainment on the western and eastern flanks of the crest, and a warm-core ring stream interaction, account for 15–30% of the total data variance for all variables. Only 18% of the zooplankton variability is due the large-scale Gulf Stream front, while 50% of the variability can be attributed to a combination of mesoscale phenomena and diel migration. On the order of 10% of the variability in the data is due to submesoscale phenomena ( $L < 20$  km). The estimated variability associated with biological processes, other than diel migration, is 20%. The error for the terms in the variance decomposition is on the order of 5%. Copyright © 1996 Elsevier Science Ltd

\* Rosenstiel School of Marine and Atmospheric Science, University of Miami, 4600 Rickenbacker Causeway, Miami, FL 33149, U.S.A.

† Present address: Department of Biology, WHOI, Woods Hole, MA 02543, U.S.A.

‡ Graduate School of Oceanography, University of Rhode Island, South Ferry Rd, Narragansett, RI 02882, U.S.A.

## 1. INTRODUCTION

In the western North Atlantic the Gulf Stream delineates a sharp boundary in both physical and biological properties. Large horizontal gradients exist across the Gulf Stream in temperature and salinity, as well as in the biomass and species composition of phytoplankton and zooplankton communities (e.g. Grice and Hart, 1962; Hurlburt, 1964; Allison and Wishner, 1986; Wishner and Allison, 1986; Ashjian and Wishner, 1993a; Ashjian *et al.*, 1994). The gradients persist even as large volumes of Gulf Stream, Sargasso Sea, and Slope Water are exchanged across the front by mesoscale features such as warm- and cold-core rings (Olson, 1991), shingles, and streamers (Garfield and Evans, 1987; Lillibridge *et al.*, 1990). Gulf Stream and Slope Waters are also exchanged along isopycnal surfaces as meanders propagate downstream from Cape Hatteras. The dynamics of Gulf Stream meanders are similar to those found in atmospheric jets, with upwelling and downwelling occurring along isopycnal surfaces in regions of divergence and convergence, respectively (Newton, 1978; Garvine, 1988). Upwelling and downwelling motions along density surfaces in the Gulf Stream are on the order of  $10 \text{ m day}^{-1}$  (Bower and Rossby, 1989), comparable to those in coastal upwelling zones.

The physical forcing associated with meanders has important consequences in the distribution and productivity of the plankton in the Slope Water and Gulf Stream. The vertical motion along density surfaces of the upper pycnocline in the Gulf Stream influences plankton distributions along the Stream front (Flierl and Davis, 1993; Olson *et al.*, 1994). "Passive" plankton species are mixed across the front near meander crests (high pressure, anticyclonic, northward excursions) and troughs (low pressure, cyclonic, southward portions of the meander). This cross-stream exchange of populations indigenous to the Slope Water and the Gulf Stream makes the meander environment a site of intense interactions between expatriate species and hostile environmental conditions from both the physical (temperature and salinity) and biological (food and competition) view point. Additionally, the upwelling of "new" nutrients into the euphotic zone in meander crests stimulates productivity, thereby enhancing phytoplankton biomass (Flierl and Davis, 1993). For macro-zooplankton, these processes primarily influence the distribution of populations through dilution or aggregation, since a reproductive response to the enhanced phytoplankton biomass that would result in a detectable change in zooplankton biomass requires timescales longer than the 5–7 days associated with the transit time of a water parcel through a meander (Mackas and Boyd, 1979; Okubo, 1980; Mackas *et al.*, 1985; Flierl and Davis, 1993; Olson *et al.*, 1994).

In September and October 1988 a two-ship study examined the structure of a meander crest of the Gulf Stream. Physical properties were examined under the Anatomy of a Meander experiment, and the plankton observations were conducted as part of the ONR-sponsored BIOSYNOP study. One experimental objective is to interpret the spatial distribution of phytoplankton and zooplankton biomass in relation to the physical structure and dynamics of the meander. A working hypothesis is that plankton biomass would show spatial patterns which reflect the net effects of cross-stream advection and nutrient input due to upwelling. The experimental design was to follow the meander for approximately one month, and observe time-dependent changes in the physical structure and plankton distributions. The adaptive feature-based sampling locations were determined from quasi-real time satellite images as well as ship and shore-based dynamical and statistical model results (see Hitchcock *et al.*, 1993).

The R.V. *Endeavor* mapped the meander crest in successive triangular sections (Hummon *et al.*, 1991), and the R.V. *Cape Hatteras* conducted transects across the main thermal front. At any given time during the experiment, in order to maximize the area over which significant estimates of the field variables could be mapped, the two ships sampled different parts of the meander crest. The density and pigment fields (Hitchcock *et al.*, 1993; Lohrenz *et al.*, 1993), and the spatial distribution of selected zooplankton species and biomass (Ashjian, 1993; Ashjian *et al.*, 1994) have been described. In general, the chlorophyll *a* distribution is strongly related to the structure of the Gulf Stream front with concentrations  $> 0.4 \text{ mg m}^{-3}$  near, or inshore of, the north wall. Characteristic length scales of pigment biomass, determined from the horizontal and temporal correlation function, are on the same order (50–100 km) as those of the physical variables. The maximum chlorophyll concentrations in the vertical coincided with the deepening of the upper pycnocline, corresponding to the 24.4–25.7  $\sigma_\theta$  surfaces, from the western (surface to 50 m) to the eastern (depths of 75–100 m) flank of the meander crest. It is concluded that the primary physical mechanisms which influenced the mesoscale pigment distribution in the anticyclonic meander are the meander-induced upwelling of nutrients along sloping isopycnals, and a Gulf Stream ring interaction.

Both the spatial distributions of zooplankton biomass and the relative proportions of Slope Water and Gulf Stream copepod species reflect the effects of cross-stream advection. Elevated levels of zooplankton biomass are found to the north and east of the meander crest, where Slope Water is entrained with characteristically high zooplankton biomass (Ashjian *et al.*, 1994). The relative proportions of two indicator species, one characteristic of the Sargasso Sea/Gulf Stream (*Pleuromamma gracilis*) and one of the Slope Water (*P. borealis*) corresponds strongly with known advective processes (Ashjian, 1993). The Gulf Stream species is numerically dominant, relative to Slope Water species, up to 80 km north of the Gulf Stream axis on the northern and western sides of the meander crest, where advective loss of Gulf Stream water occurs. Slope Water species, in contrast, are numerically dominant at all locations north of the Stream axis on the northeastern side of the crest, consistent with the entrainment of Slope Water into the Gulf Stream at that location.

While previous reports have described plankton biomass distributions in detail, there has been no quantitative assessment of temporal and spatial variability. The primary goal of this study is to describe quantitatively the variability by a principal component analysis of the hydrographic data, chlorophyll *a*, and zooplankton biomass in a meander-following curvilinear coordinate system (Section 2.1). Principal Component Analysis (PCA) has been extensively utilized in analysis of physical fields (Preisendorfer, 1988). PCA was first applied to spatial distributions of marine plankton populations by Blasco (1971) and Denman and Platt (1978). The technique has since been used to describe the spatial and temporal variability of several biological parameters in the ocean (e.g. Jassby and Powell, 1990; García-Moliner *et al.*, 1993). Here, spatial maps of Principal Components (PCs) in a meander-based coordinate system, the temporal distribution of PCs, and the vertical statistical modes are discussed to interpret the time-varying spatial distributions in relation to dynamics of the meander (Section 3).

## 2. METHODOLOGY

The physical variables for the PCA are taken from 409 temperature profiles from XBTs and CTDs, and 201 salinity and density profiles from lowered CTDs and a MOCNESS. The

corresponding 90 fluorescence profiles from CTD casts taken on the R.V. *Endeavor* are converted to total chlorophyll *a* concentrations by least-squares regression against discrete samples, as described in Hitchcock *et al.* (1993). A detailed description of the data and an analysis of the dynamical events during the meander crest experiment form part of Hummon's (1995) doctoral dissertation. Processing details, station locations, profile plots, and auxiliary data are in Hummon *et al.* (1991). The zooplankton biomass is estimated from volume backscatter data from an acoustic Doppler current profiler mounted in the hull of R.V. *Cape Hatteras*. The number of zooplankton biomass data points used for analysis ranged from 3572 to 5253 for 10 m intervals between 20 and 120 m (Ashjian *et al.*, 1994).

Two factors restricted the depth interval for the PCA to 20–120 m. First, the number of data points decrease towards the surface from 20 m, especially for zooplankton biomass. Second, the variability of the physical fields decreased rapidly in the mixed layer (upper 20 m). The lower limit of 120 m is selected as it is the lower limit of the significant chlorophyll *a* (chl *a*) signal (Mariano and Hitchcock, 1993) and the error in the zooplankton biomass estimates also increases with depth. A separate analysis, which included data to depths of 230 m, did not alter the observed patterns.

### 2.1. *The curvilinear coordinate system*

The interpretation of the distribution of the principal components is greatly simplified by utilizing a local stream-based curvilinear coordinate system. The origin of this system is defined by the position of the apex of the meander crest. The along-stream coordinate values are calculated from daily objective analysis maps of the depth of the 12° isotherm,  $Z_{12}$ , constructed according to the parameter matrix objective analysis algorithm (Mariano and Brown, 1992) with > 500 temperature measurements from CTD, XBT, and AXBT deployments; these include several temperature observations outside the region analyzed in the PCA. Each  $Z_{12} = 400$  m contour on a given day serves as a basis for the along-stream coordinate,  $\tau$ , in km. The primary reason that this contour is chosen as a reference isotherm is that it remained connected (i.e. intact) during stream ring interactions; hence, the coordinate system topology did not change during the analysis. This contour corresponds to the nominal location of the maximum cyclonic horizontal velocity shear in the main thermocline of the Gulf Stream as determined by Halkin and Rossby (1985) from the PEGASUS data at 73°W. There is a well-known shoreward offset of 14–15 km between the surface front, defined as the maximum gradient in sea surface temperature, and the subsurface front (Hansen and Maul, 1970; Cornillon and Watts, 1987), defined by either  $Z_{12} = 300$  m or  $Z_{15} = 200$  m. A deeper front indicator,  $Z_{12} = 400$  m, is used here for the  $\tau$  coordinate. Consequently, the near-surface property fronts should be displaced on the order of 20–25 km shoreward in our coordinate system.

The  $\tau$  values are stored as daily files which contain longitude, latitude, and the along-stream coordinate distance,  $(x, y, \tau)$ , respectively. In each file the origin of the along-stream coordinate,  $\tau = 0$ , is set at the apex of the meander crest. The  $\tau$  values are the distance along the  $Z_{12} = 400$  m contour and are calculated relative to the apex as differences in longitude and latitude between the apex and the set of  $Z_{12} = 400$  m contour positions on a Mercator projection. Negative  $\tau$  values are upstream of the apex, i.e. west of the apex of the meander crest, while positive  $\tau$  values are downstream, east of the meander apex.

The origin of the cross-stream coordinate,  $\eta = 0$  km, is defined at  $Z_{12} = 400$  m. Negative  $\eta$  values correspond to Gulf Stream core and Sargasso Sea locations, while positive  $\eta$  values

correspond to North Wall and Slope Water locations. A brute-force search technique is used for calculating the  $\tau$  and  $\eta$  values for the  $j$ th profile. Two daily files that bracket the  $j$ th profile in time are selected. For each daily file, the point  $(x, y)$  closest to the location of the profile is found by calculating all possible distances, defined by the usual  $L_2$  norm, and selecting the minimum distance. This yields two estimates of  $(\tau, \eta)$ , one from each daily file, which are then averaged using linear weights based on the time differences between each daily file and the time of the  $j$ th profile. The nominal location of the North Wall, here defined as  $Z_{12} = 300$  m, is  $\eta = 25$  km. This coordinate system has been used to interpret zooplankton biomass and species distributions about the meander (Ashjian, 1993; Ashjian *et al.*, 1994), and the spatial distribution of productivity (Lohrenz *et al.*, 1993). An Objective Analysis (OA) map illustrating this coordinate system is shown in Fig. 16(a).

## 2.2. Cross-sectional averages

The average cross-sections of each variable are calculated with a smooth two-dimensional bicubic spline fit to the data in a cross-stream, depth  $(\eta, z)$  coordinate system. For each variable  $Q$ , bicubic spline coefficients are fitted to all data  $Q_{ij}$  using  $\eta$  estimated by the brute-force technique from the time, longitude, and latitude of the  $j$ th profile (Section 2.1). The depth,  $z$ , is related to the  $i$ th analysis level by  $z = 10(i - 1) + 20$  m. The calculations of the spline coefficients and the evaluation of the spline trend surface using these coefficients are performed, by their respective ranges, in a normalized  $(\eta, z)$  coordinate system to avoid ill-conditioned inversions owing to the thousand-fold difference in horizontal (km) and vertical units (m).

The spline parameters of the smoothing splines are empirically determined to subjectively partition the mean and varying fields. The objective is to explain a majority of cross-stream variance by the average cross-sections; this is necessary to ensure that the investigation of the more subtle along-stream variability is not compromised by the presence of the greater cross-stream variability. However, since data with a large range of temporal and along-stream locations are binned only by cross-stream distance in the spline fit, a tight spline fit with small root-mean-square fitting (or interpolating) error leads to a mean cross-section with undesirable large-amplitude, high wavenumber components. The spline parameters are set first by starting with smooth splines (high rms fitting error) and then by adjusting the smoothness parameter for a low rms fitting error and minimal high frequency oscillations for the density and temperature trend.

The same set of spline parameters is used for all variables. The alternative would be to tune the spline parameters for each variable, but doing this would make comparisons of the cross-stream trend surfaces difficult. The only problem we have noted with using all the same spline parameters is with the zooplankton mean cross-section. Most of the zooplankton samples were collected near the front, and there are relatively sparse measurements in the Gulf Stream core. The splines extrapolate from a region with large gradients into a more homogeneous region with sparse measurements. Consequently, the zooplankton biomass is over-estimated at the deeper depths on the Gulf Stream side. Also, as with all decompositions of finite and noisy data into different components, there will be leakage between scales, and this is evident in our spline fits (Figs 3 and 4), which explain 80%, 80%, 54%, 50%, and 18% of the variance in the average cross-sections of density, temperature, salinity, chlorophyll *a* and zooplankton data, respectively. On the other hand, given our one month sampling of these fields and the fact that the cross-stream advection of

passive tracers by secondary circulations is always present in the meander crest, one can argue that the smaller scale features evident in Figs 3 and 4 are always present in the data and should be represented in the average cross-stream structure of these fields.

### 2.3. Principal component analysis

The geometric interpretation of a PCA is first to translate all data about the data centroid and then to rotate the coordinate system such that the first coordinate is in the direction of maximum variability. The second coordinate in the newly-translated and rotated coordinate system is then set in the orthogonal direction to explain the maximum amount of remaining variability, and so on. The power of PCA lies in the ability to identify the most efficient basis for representing the data, and thereby determine the dominant patterns of spatial and temporal variability. However, this power is easily abused (Richman, 1986). The data sampling may determine the shape of the dominant statistical patterns and thereby corrupt any dynamical analysis based on these patterns. The results presented in Section 3 indicate that in our analysis these problems are minimal.

The PCA is formulated as follows: let  $Q_{ij}$  denote any of the analysis variables (temperature, salinity, density, chl *a* or zooplankton biomass) from the  $j$ th station (or profile) and  $i$ th depth. The data are specified at  $n$  depths, and for our analysis  $n = 11$ . Let  $\bar{Q}_{ij}$  denote the value of the corresponding bicubic spline trend surface evaluated for the  $i$ th depth, denoted here by  $z$ , and  $j$ th profile by first calculating the cross-stream distance  $\eta$  using the longitude, latitude and time of the  $j$ th profile and the brute-force search technique described in Section 2.1. The  $z$  and  $\eta$  values of the  $j$ th profile are used with the precalculated spline coefficients for determining the trend value,  $\bar{Q}_{ij}$ , that is needed for detrending the data for the depth covariance calculations.

The ordered eigenvectors,  $\mathbf{E}_1$ , corresponding to the ordered ( $\lambda_1 > \lambda_2 > \dots$ ) eigenvalues  $\lambda_l$ , of the depth covariance matrix of  $\mathbf{Q}$ ,

$$\begin{pmatrix} \langle (Q_{1j} - \bar{Q}_{1j})^2 \rangle & \langle (Q_{1j} - \bar{Q}_{1j})(Q_{2j} - \bar{Q}_{2j}) \rangle & \cdots & \langle (Q_{1j} - \bar{Q}_{1j})(Q_{nj} - \bar{Q}_{nj}) \rangle \\ \vdots & \vdots & \vdots & \vdots \\ \langle (Q_{nj} - \bar{Q}_{nj})(Q_{1j} - \bar{Q}_{1j}) \rangle & \cdots & \cdots & \langle (Q_{nj} - \bar{Q}_{nj})^2 \rangle \end{pmatrix},$$

are the most efficient basis for representing the data. The expected value operator,  $\langle \rangle$ , is estimated by an arithmetic average of all the profiles, i.e. an average over the index  $j$ .  $\mathbf{E}_1$  are the "statistical" vertical modes that the data are decomposed into. The value for the  $i$ th depth from the  $j$ th profile can be expressed from a linear sum of the cross-stream trend  $\bar{Q}_{ij}$ , the  $n_{sig}$  significant eigenvectors  $\mathbf{E}_1$  multiplied by the square root of the corresponding eigenvalues  $\lambda_l$ , and noise,  $\varepsilon_{lj}$ ,

$$Q_{ij} = \bar{Q}_{ij} + \sum_l^{n_{sig}} pc_{lj} E_l \sqrt{\lambda_l} + \varepsilon_{lj}, \quad j = 1, 2, \dots$$

The  $pc_{lj}$  are calculated from a least-squares fit over  $i$  for each  $j$  using the  $n_{sig}$  vertical eigenvectors as the set of independent regression variables. These regression coefficients are known as principal components (or modal amplitudes) of the  $l$ th eigenvector for the  $j$ th profile. For each vertical eigenvector  $E_l$ , there is one principal component for each station and for each variable. After an examination of the average statistics in Section 3.1, and the

normalized vertical eigenvectors, known as empirical orthogonal functions (EOFs), in Section 3.2, the spatial and temporal distribution of the set of principal components corresponding to the first two eigenvectors for each of the analysis variables are investigated in Section 3.3.

In the following sections, many curves and patterns will be compared. Most of these comparisons are visual because there is no simple acceptable statistical measure for pattern matching, especially for those representing complicated physical and biological fields that are found in the Gulf Stream ring and meander region. We will use the word similar when two curves or two sets of patterns have extrema occurring in the same region, gradients are of almost equal magnitude, and the boundaries of the primary features have approximately the same shape. See the discussion by Mariano (1990) on the use of these attributes for determining similar fields.

### 3. RESULTS

#### 3.1. First- and second-order statistics

The average vertical profiles and corresponding cross-sections for each of the five variables are shown in Figs 1–4. The three physical properties of interest, temperature, salinity, and density, show the expected vertical gradients, while the corresponding variance profiles identify the regions of either maximum horizontal property gradients or vertical displacements of property fields with large vertical gradients. As expected, density increases with depth. The maximum vertical density variance occurred between 80 and 90 m while the

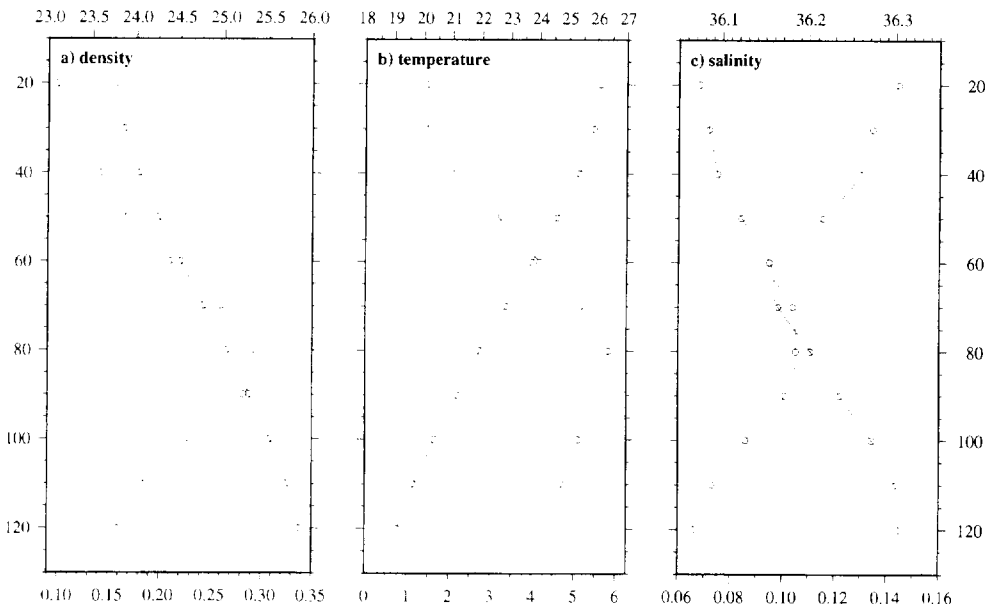


Fig. 1. The average vertical profile for (a) density ( $\text{g}/\text{cm}^3$ ), (b) temperature ( $^{\circ}\text{C}$ ) and (c) salinity ( $\text{g}/\text{kg}$ ) and their variances ( $\text{g}^2/\text{cm}^6$ ,  $^{\circ}\text{C}^2$ , and  $\text{g}^2/\text{kg}^2$ , respectively). Averages are denoted by solid lines and are scaled on the top axis. Variances are denoted by dashed lines and are scaled on the bottom axis. The vertical axis is depth in meters.

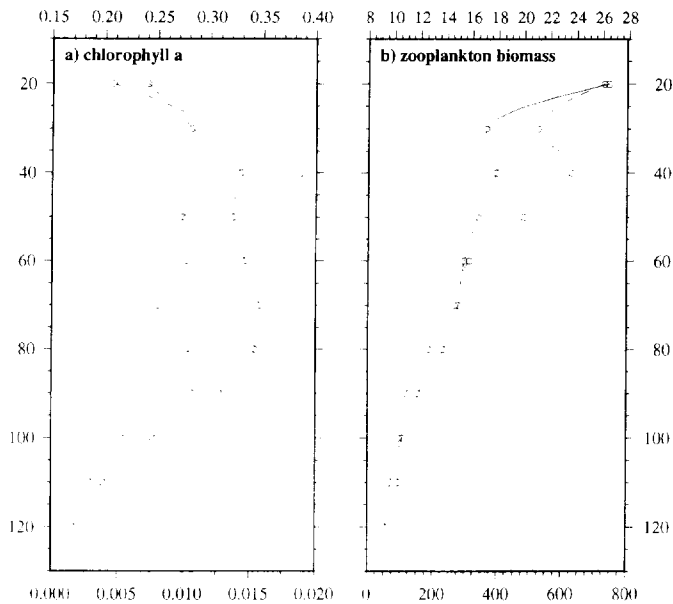


Fig. 2. Like Fig. 1 but for (a) chlorophyll *a* ( $\text{mg}/\text{m}^3$ ) and (b) zooplankton biomass ( $\text{mg}/\text{m}^3$ ).

minimum variance is near the surface (Fig. 1(a)). Temperature decreases with depth, with the minimum variance near 25 m and the maximum variance near 80 m (Fig. 1(b)). This pattern indicates the mixed layer is less than 25 m deep across the width of the transects (see figures in Hitchcock *et al.*, 1993). The increase in variance between 30 m and 80 m corresponds to the shoaling/deepening of the seasonal thermocline. The salinity profile, in contrast, shows maximum variability near the surface. The average salinity profile had the most curvature of the three physical variables (Fig. 1(c)), reflecting the large gradient in surface salinity between the Sargasso Sea and the Slope Water. Figure 1 clearly illustrates a tighter coupling between temperature and density than between salinity and density. This and the fact that surface forcing of the salinity field is relatively weak make salinity a good tracer of cross-meander mixing (see Olson, 1986).

The vertical patterns of the two plankton biomass indices are similar in one respect: the average vertical distribution and the variance for both phyto- and zooplankton have the same overall tendencies. This is especially true for the zooplankton biomass distributions—both curves have maxima at 20 m, local minima at 30 m, local maxima at 40 m, and an almost monotonic decrease to a minimum at 120 m. The phytoplankton distributions both have local maxima at 40 m that decrease toward the surface, a fairly homogeneous layer between 50 and 90 m, and a monotonic decrease to 120 m. The close agreement between the mean and variance distributions is an expected outcome if the rates are auto-catalytic, i.e.  $dN/dt \propto N$ .

The average vertical profile of chlorophyll *a* indicates that in the mean, the subsurface pigment maximum occurred between 40 and 90 m (Fig. 2(a)). The maximum variance between 40 and 90 m corresponds to the depth range over which the subsurface maximum is observed (Hitchcock *et al.*, 1993). The peak in chlorophyll *a* variance at 40 m, in particular, corresponds to the top of the seasonal thermocline. On average, zooplankton biomass is highest near 20 m, the base of the mixed layer, where maximum variance is also found (Fig.

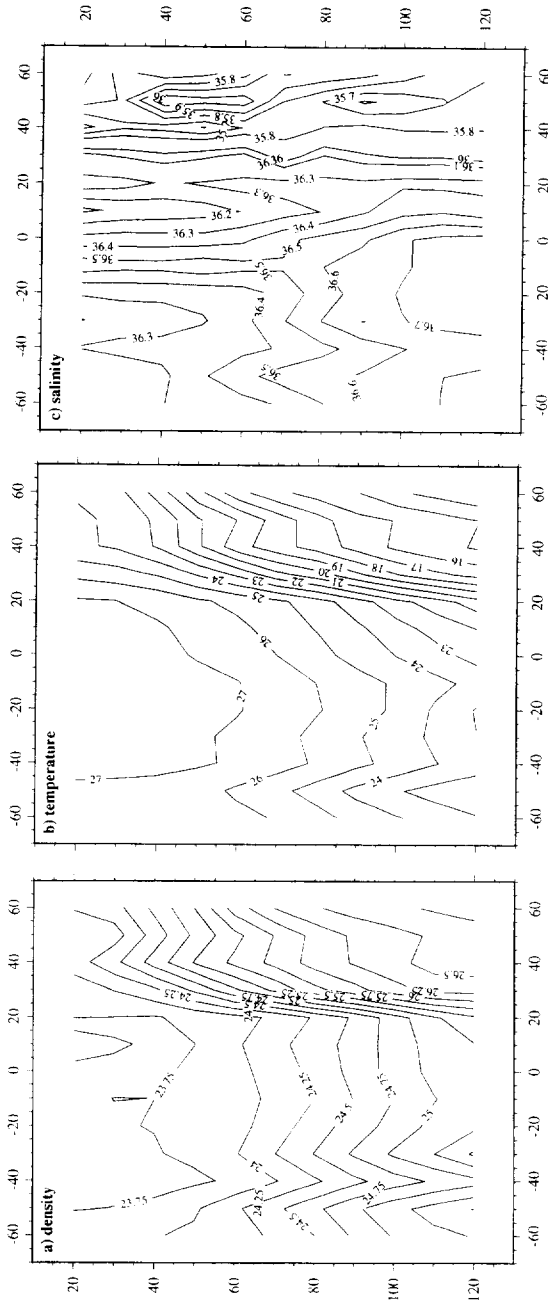


Fig. 3. The average cross-sections for (a) density, (b) temperature and (c) salinity. Vertical axis is depth in meters. Horizontal axis is cross-stream distance in km. Slope water locations are at cross-stream distances greater than 30 km, the Sargasso Sea side of the Gulf Stream is at negative cross-stream distances.

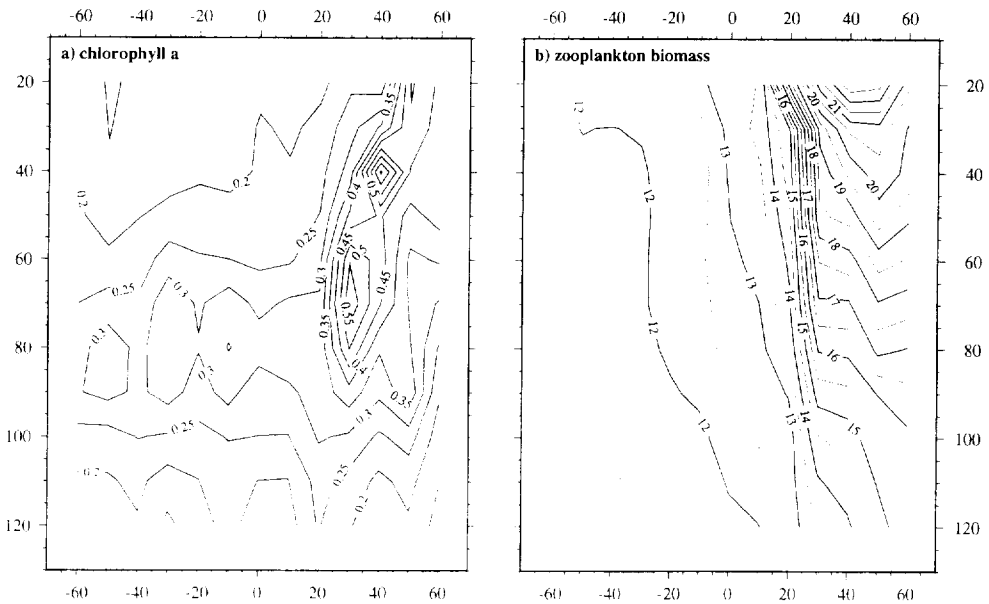


Fig. 4. Like Fig. 3, but for (a) chlorophyll *a* and (b) zooplankton biomass.

2(b); see also Ashjian *et al.*, 1994). The high variance near the surface may be associated with the cross-stream gradient in biomass, with an order of magnitude greater biomass in the Slope Water than in the Sargasso Sea (Ashjian *et al.*, 1994). Another important influence may be diel vertical migration, which results in an increase in biomass within the upper water column at night thus adding a diurnal variability component to the variance field. The PCA, presented below, indicates both are important.

The mean cross-stream sections (Figs 3 and 4) account for  $\approx 20\text{--}80\%$  of the total variability in each of the five variables. The property fronts for four of the variables occurred at cross-stream distances of 20–40 km with maximum gradients at 25–30 km. The surface zooplankton front, in contrast, is displaced 5–10 km seaward of the physical and chlorophyll *a* fronts (Fig. 4(a),(b)). A similar seaward offset, relative to phytoplankton biomass and physical fronts, was detected for zooplankton biomass in a filament in the Coastal Transition Zone off Pt Arena in 1988 (e.g. Chavez *et al.*, 1991; Mackas *et al.*, 1991; Strub *et al.*, 1991).

The local extrema in density (Fig. 3(a)) coincided well with local extremum in temperature (Fig. 3(b)) and salinity (Fig. 3(c)) associated with the tropical/subtropical advective core of the surface Gulf Stream. Given that there are twice as many temperature profiles as there are of salinity and density, and that the data are taken from a very heterogeneous and nonstationary environment, this agreement strengthens the interpretation of the bi-cubic spline fits as cross-sectional trends.

As expected, the mean property sections show the cooler, fresher Slope Water north of the Gulf Stream. Conversely, warmer, saltier waters occurred at the southern edge of the Gulf Stream. The thermocline–pycnocline shoaled along the northern edge of the Gulf Stream, as evidenced by the high horizontal gradients in the property fields within 30 km of the large cyclonic shear region (0 km) of the Gulf Stream core. As with the vertical averages and variances, there is a tighter agreement between temperature and density than with salinity

and density. If salinity is interpreted as a “passive” tracer, i.e. an indicator of mixing, the secondary fronts at  $\eta = -10$  km in salinity, zooplankton, and chlorophyll *a* can be viewed as cross-frontal mixing features. These are discussed below in the context of previously reported speciation cross-sections (Ashjian, 1993; Ashjian *et al.*, 1994).

The mean chlorophyll *a* and salinity cross-sections, and to a lesser extent temperature, each contain localized maxima embedded in the larger-scale trend. The mean salinity and chlorophyll *a* surfaces explain about one-half of the respective variability, as compared to 80% for temperature and density. Only 18% of the zooplankton biomass variability is attributed to the cross-sectional fit. We hypothesize that this low percentage is due to the temporal patchiness associated with the diel vertical migration of the zooplankton.

### 3.2. Vertical empirical orthogonal functions

The remaining variability of each of the five variables is decomposed with the set of normalized vertical eigenvectors of the covariance matrix, as described above. The variance explained by each of the first two modes in the vertical, relative to the corresponding mean section, is included in the corresponding figures. The first “vertical” EOFs for temperature, salinity, and density are fairly coherent with depth, exhibiting a slight change in amplitude between 50 and 120 m (Fig. 5). The first EOFs of density (Fig. 5(a)) and temperature (Fig. 5(b)) are nearly identical with decreasing variability towards the surface mixed layer. In contrast, both salinity EOFs (Fig. 5(c)) indicate increasing variability towards the surface. The first EOFs of temperature, salinity and density explain 60–70% of the detrended

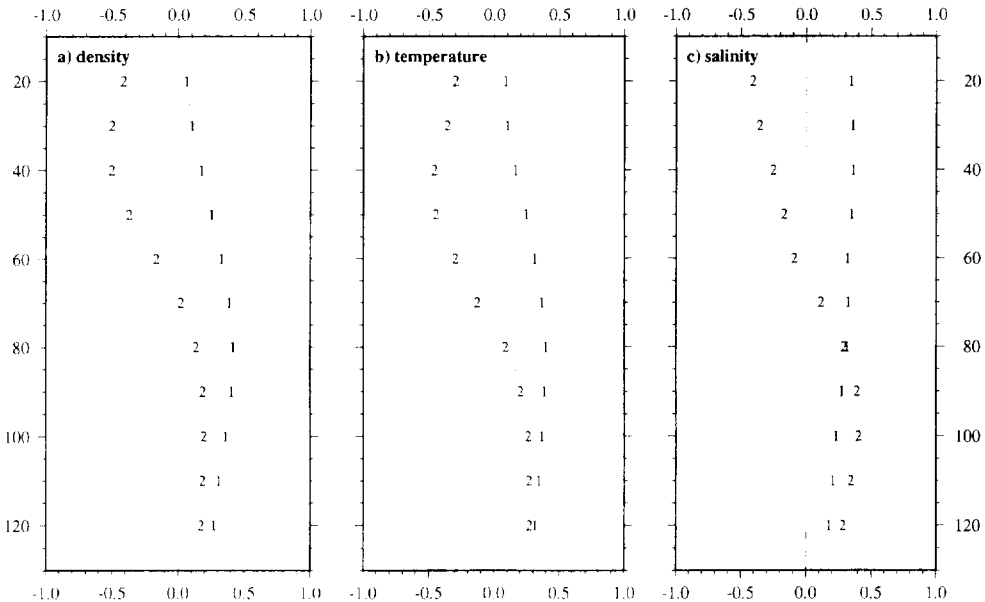


Fig. 5. The first two vertical EOFs for (a) density, (b) temperature and (c) salinity. The vertical axis is depth in m and the horizontal axis is nondimensional modal amplitude. The variance explained, relative to the mean cross-section, by mode 1 and mode 2 for density is 73.7% and 15.0%; for temperature it is 78.1% and 9.7%; and for salinity it is 60.7% and 20.6%.

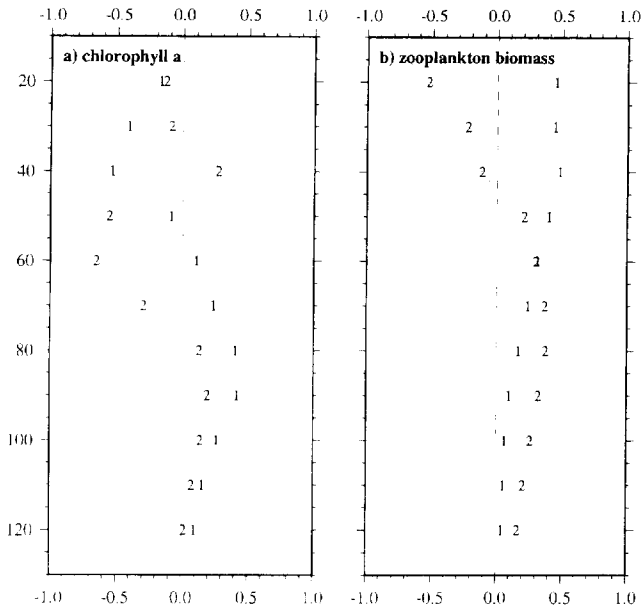


Fig. 6. Like Fig. 5 but for (a) chlorophyll *a* and (b) zooplankton biomass. The variance explained by mode 1 and mode 2 for chlorophyll *a* is 39.4% and 20.8%, and for zooplankton biomass it is 60.6% and 15.8%.

variability in the data. The second EOFs of the physical fields are similar in vertical shape to each other, and explain an additional 10–20% of the detrended data variability.

The first chlorophyll EOF, in contrast, contains a much lower proportion of the remaining variability (39%) than did those of the physical variables. This suggests that phytoplankton patchiness is manifested in the residual (from the average cross-stream section) fields, i.e. as expected, biological interactions such as grazing are also important. The first chlorophyll EOF exhibited a well-defined sign change centered about 55 m (Fig. 6(a)). We believe that the sign change is due to the fact that the subsurface chlorophyll *a* maximum is found at different depths on the western and eastern flank of the meander crest. Hitchcock *et al.* (1993) showed a strong coupling, in the mean, between chlorophyll isopleths and isopycnal surfaces between  $\sigma_{\theta} = 24.4$  and 25.7. A preliminary analysis of the data revealed no significant signal below 120 m in either of the two chlorophyll EOFs.

The zooplankton EOFs are qualitatively most similar to the EOFs of salinity, with the first two EOFs representing about 76% of the remaining variability (Fig. 6(b)). The first zooplankton mode is near-surface intensified and decreases to near zero between 40 and 120 m, while the second mode contains a sign change near 45 m. The second zooplankton EOF is similar to that of the first chlorophyll EOF, except near the surface. The horizontal patterns of the corresponding principal components are also similar in size and location, and the significance of this is discussed in the next section.

### 3.3. Analysis of the spatial and temporal distribution of principal components

The first two principal components (PCs) are calculated for each variable at each station, and subsequently mapped in the curvilinear coordinate system with the objective analysis

scheme (as described in Section 2.1). In interpreting the physical fields a positive first PC implies values greater than the mean section at all depths between 20 and 120 m, while a positive second PC implies values greater than the mean between 70 and 120 m and values lower than the mean between 20 and 70 m. A negative first PC implies values lower than the mean section at all depths, while a negative second PC implies values lower than the mean between 70 and 120 m and values greater than the mean between 20 and 70 m for the physical fields. The distributions of the first density and first temperature PCs are, in light of the different sampling of the heterogeneous and nonstationary temperature and salinity fields, remarkably similar (Fig. 7(a),(b)). The difference in sign of the PCs between the two variables is due to the fact that lower-than-average temperature, leads to higher-than-average density. Conversely, a higher-than-average temperature results in a lower density, if all other factors are equal. The distributions of the second temperature and density PCs consist entirely of relatively low amplitude values (Fig. 7(a),(b)). The PC distributions of these two variables, as well as the similarity of the EOF modes, the vertical variance estimates, the eigenvalues of the covariance matrix, and the vertical and cross-sectional averages, indicate that variability in temperature is more important than that of salinity in determining the variability of the density field.

Salinity (Fig. 7(c)) and chlorophyll *a* (Fig. 8(a)) exhibit similar, but inverse, patterns of variability. This inverse relationship is expected. For example, low salinity Slope Water is characterized by high chlorophyll *a* biomass, in contrast to the saltier Gulf Stream core water which is characterized by low chlorophyll *a* biomass. Both fields have similar eigenvalues, and the cross-sections contain more evidence of smaller-scale features than did the cross-sectional fields of temperature and density. Furthermore, the variance explained by the decomposition in salinity and chlorophyll *a* is similar. The tight coupling observed between temperature and density, and the similarity in the salinity and chlorophyll variability, reinforces the hypothesis that salinity behaves as a passive tracer.

The interpretation of the zooplankton biomass fields is similar to that of the physical fields since their EOFs are similar. Hence, positive first PCs imply greater than average biomass at all depths, while positive second PCs imply values lower than the mean above 45 m and values greater than the mean at depths below 45 m. The magnitudes of the first two PCs varied across the meander (Fig. 8(b)). The first principal component indicates that greater-than-average biomass is observed north of the Gulf Stream axis on both sides of the meander crest, especially on the eastern flank north of the North Wall. The high biomass to the south of the Stream axis is an artifact of the sampling and analysis techniques; computation of the mean zooplankton biomass distribution, EOFs, and PCs is done on all data, regardless of time of day. Examination of the cruise track and associated times of day revealed this section of the meander was surveyed only at night, so the enhanced biomass resulted from an increase in biomass as a result of diel vertical migration (Ashjian *et al.*, 1994). The day-to-night ratio is 2:1 on the average between 20 and 120 m. A separate analysis is performed for the day and night data in Section 3.4.

The second principal component for zooplankton biomass has a distribution similar to the first on the eastern side of the crest with a slight seaward displacement of the primary variability pattern; however, lower values are found on the western side of the crest (Fig. 8(b)). It is striking that the largest positive values are observed for both principal components in the region to the north and east of the meander crest.

There is also a similarity between the spatial pattern of the second principal component of zooplankton biomass with the spatial pattern of the first principal component of

phytoplankton biomass. The primary difference between these two patterns is that the maximum zooplankton variability is shifted downstream of the maximum phytoplankton biomass. This shift may reflect the discontemporaneous collection of the zooplankton and chlorophyll data: the chlorophyll data (collected on the R.V. *Endeavor*) was collected approximately 1 week earlier than the zooplankton data (on the R.V. *Cape Hatteras*). Hence the increased variability may in fact represent the same feature that has simply been advected further downstream. A second explanation may lie in the different mechanisms that influence zooplankton and chlorophyll variability. Chlorophyll should be elevated in response to upwelling on the western side of the crest, although the elevation would not be observed until further advection downstream (Flierl and Davis, 1993). In contrast, zooplankton variability may be altered primarily by physical mechanisms (advection, concentration, dilution) which would concentrate biomass or advect high biomass in from the Slope Water on the eastern side of the crest. However, the manifestation of these two mechanisms need not be spatially coincident.

The first PCs of all the data are shown as a function of cross-stream distance in Fig. 9. For all variables, the variability in the Slope Water is much greater than that in the Stream. In general, the enhanced variability envelope occurs at cross-stream distances between 10 km and 60 km. For salinity, however, extreme PC values are also evident in the Gulf Stream core (Fig. 9(c)). The distribution of all of the chlorophyll *a* PCs as a function of along-stream distance reveals an enhanced signal on the eastern side of the meander (Fig. 10) potentially in response to upwelling of nutrients along the western flank (see Discussion).

The temporal distributions of the PCs are investigated as a function of cruise duration and time of day. The only obvious signal in the 20 distributions (two temporal distributions  $\times$  5 variables  $\times$  2 modes) is the daily zooplankton PC distribution for the first mode (Fig. 11). This temporal distribution indicates that the first zooplankton EOF is influenced by diel migration. This first mode explains about 50% of the *over all* variability contained in the zooplankton data set. The largest positive PC values occurred between sunset and sunrise with a sharp decline approximately 1/2 h before sunrise. The very large ( $> 3.0$ ) PC values represent high zooplankton biomass in the Slope Water far north of the meander. The lack of a diel pattern in the pigment data is interpreted as an indication that pigment biomass is minimally influenced by any diel periodicity in the fluorescence per unit chlorophyll *a*.

#### 3.4. Analysis of day and night zooplankton data

Because of the large diurnal signal, the zooplankton biomass data are separated into day and night data for a complete analysis of the diel variability. The mean vertical distributions demonstrate that night zooplankton concentrations are 50% greater than the day concentrations in the depth range of 20–120 m (Fig. 12). The maximum variance observed is at a depth of 40 m for the night samples (Fig. 12(a)) and is at a depth of 20 m for the day samples (Fig. 12(b)). There is a sharp peak in daytime zooplankton biomass between 30 and 20 m representing an accumulation of biomass at the base of the mixed layer. We are not able to resolve whether this peak is a result of downward movement of zooplankton to this depth during the day or whether this is a persistent feature that is masked by greater levels of biomass following upward migration of zooplankton during the night. The variance values at night are an order of magnitude larger than the values during the day over most of the depths sampled. Since the zooplankton biomass measurements did not span the entire range of daily migration, being limited to the upper water column (20–120 m), the diel vertical

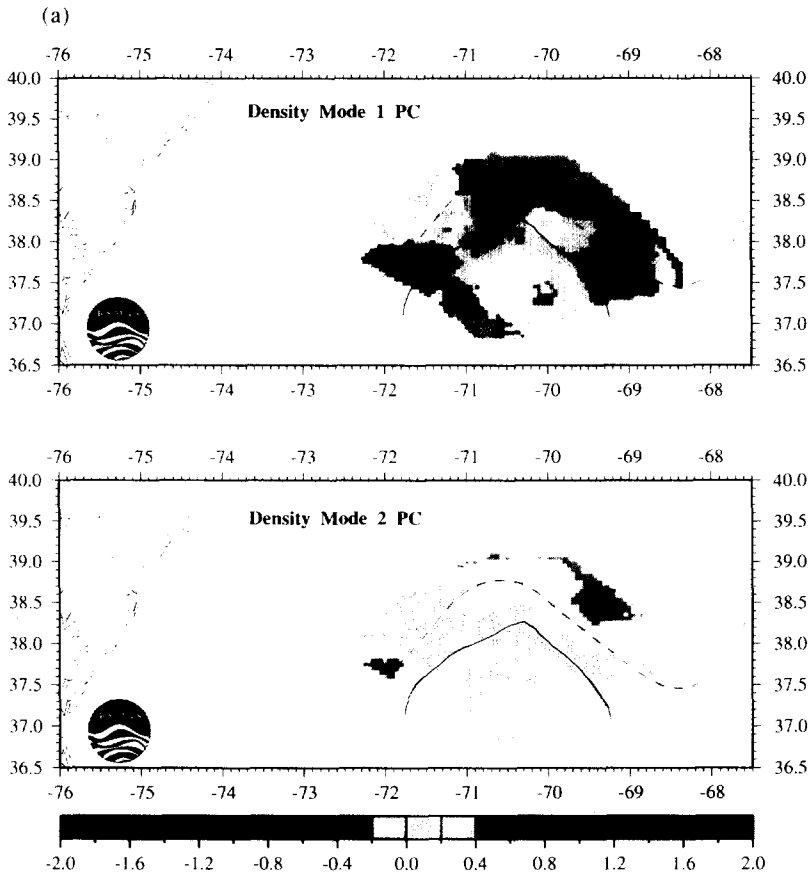


Fig. 7. (a) The spatial distribution of the first (top panel) and second (bottom panel) principal components for density plotted at an arbitrary average location. The dashed line is the Gulf Stream North Edge position for day 271 provided by Chin and Mariano (in press). The solid line is the location of the  $12^{\circ}\text{C}$  isotherm at 400 m from the corresponding objective analysis map. The solid line corresponds to a cross-stream distance of 0 km. (b) As (a) but for temperature. (c) As (a) but for salinity.

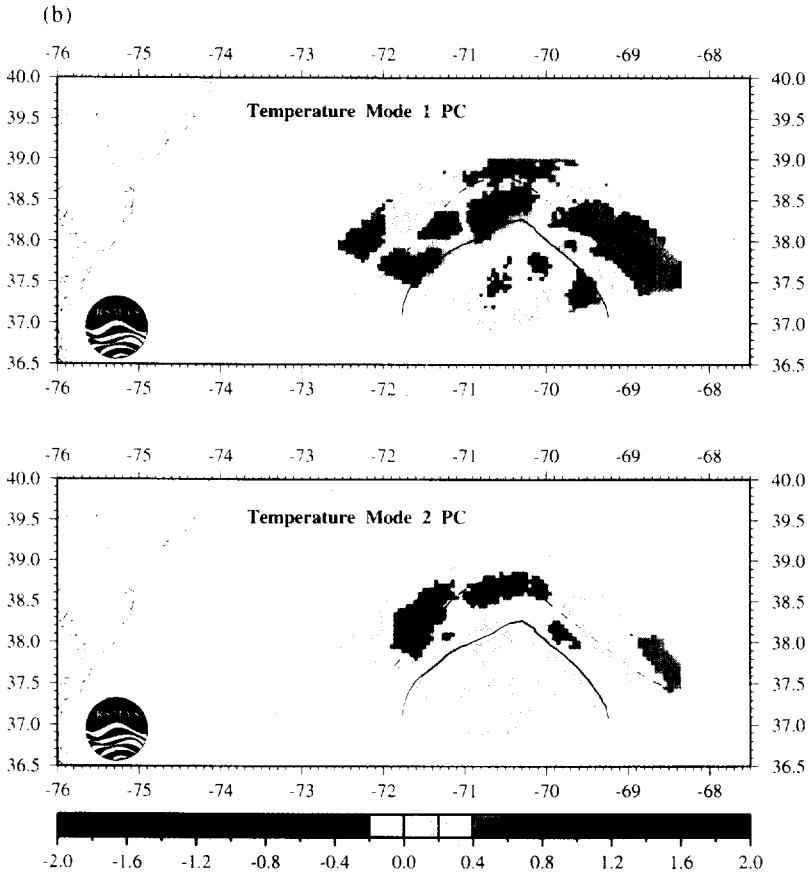


Fig. 7(b).

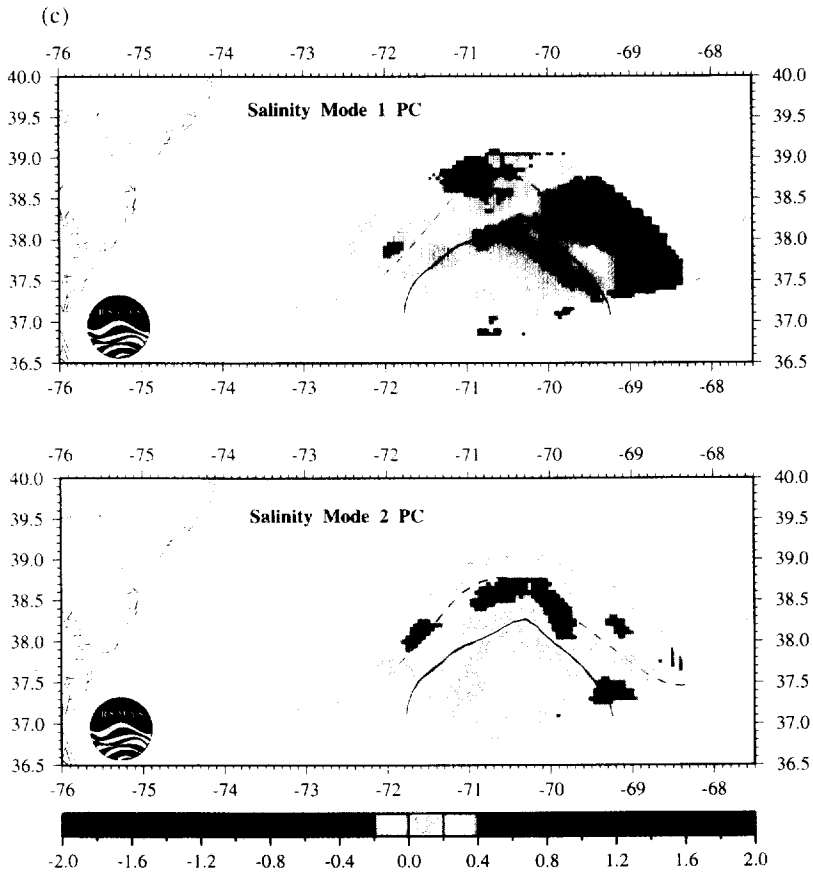


Fig. 7(c).

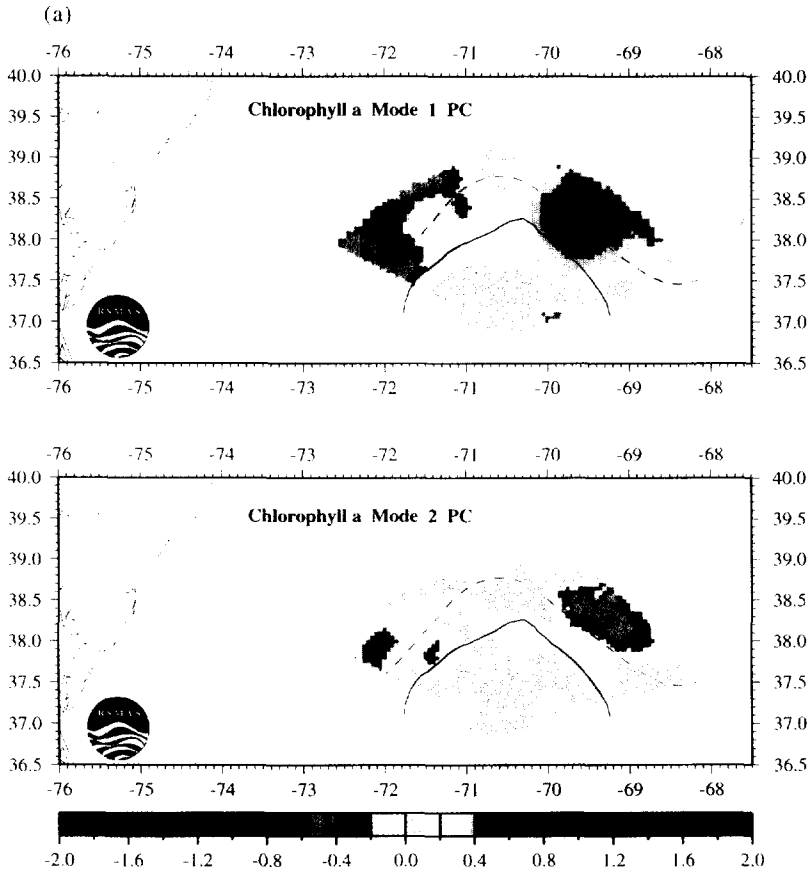


Fig. 8. Like Fig. 7(a) but for (a) chlorophyll *a* and (b) zooplankton biomass.

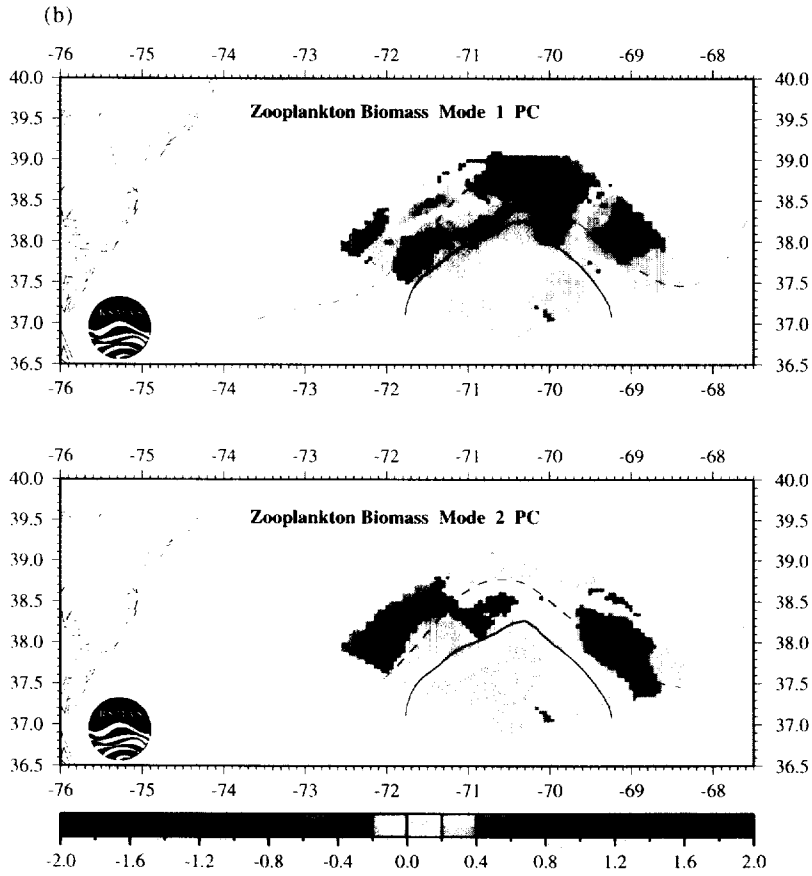


Fig. 8(b).

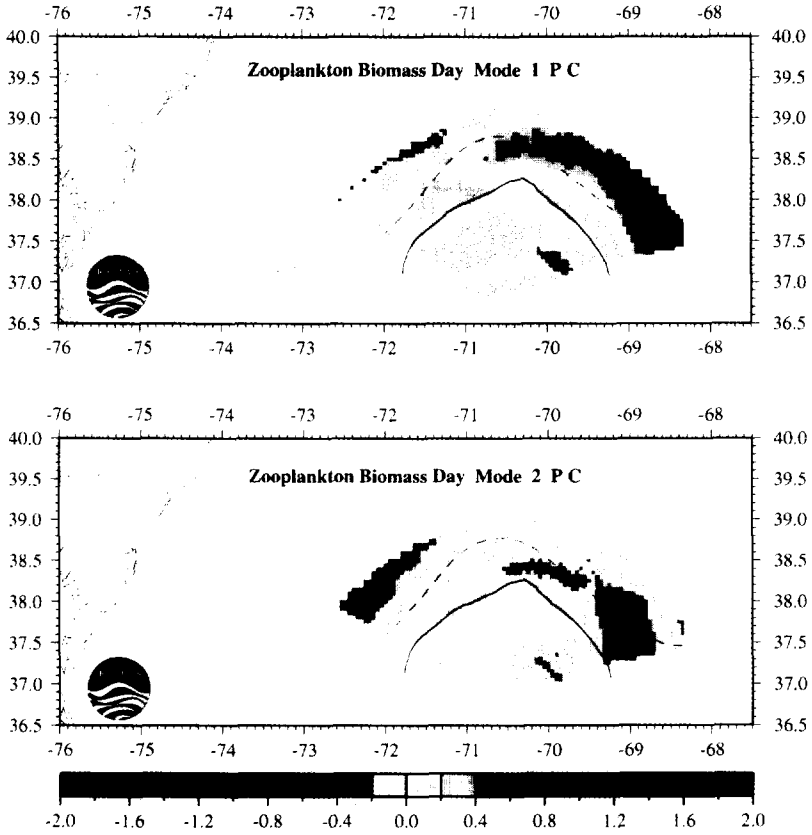


Fig. 14. Like Fig. 7(a) but for zooplankton biomass.

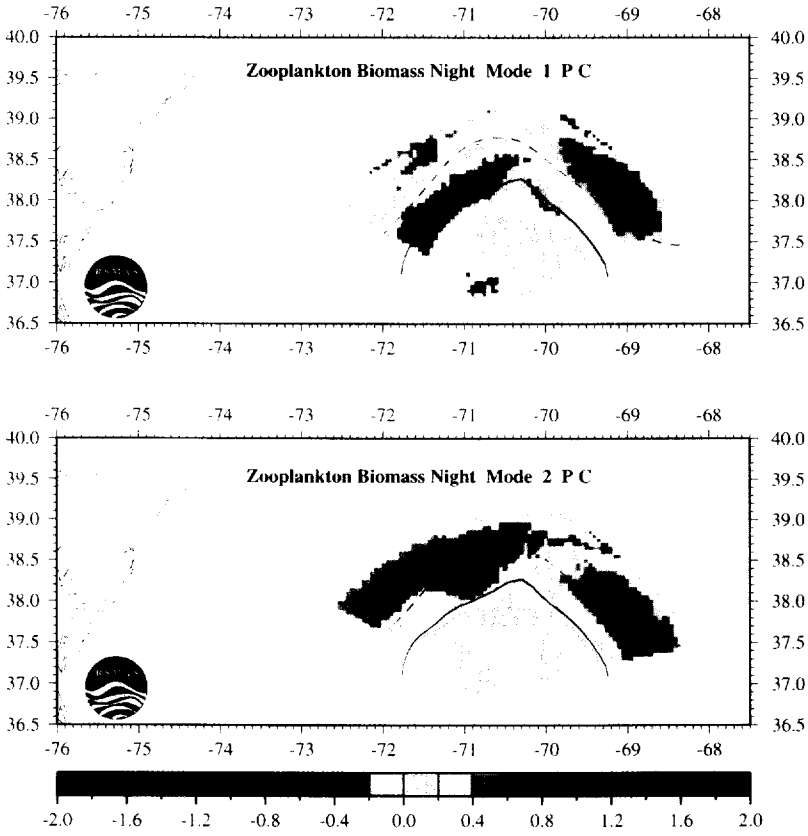


Fig. 15. Like Fig. 7(a) but for zooplankton biomass night.



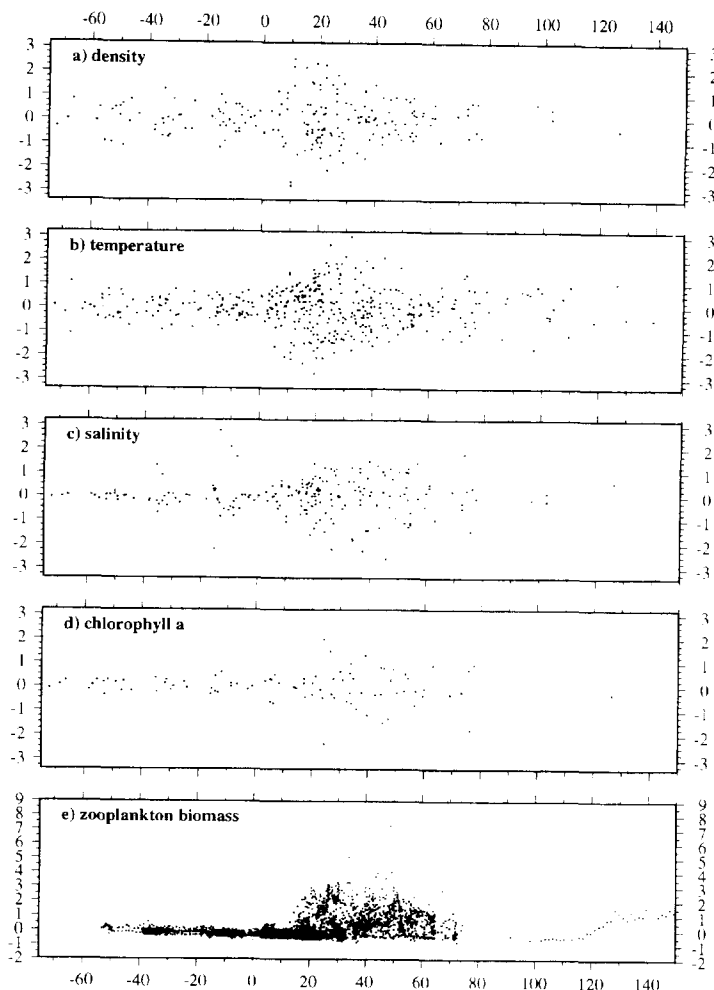


Fig. 9. The distribution of the first principal component as a function of cross-stream distance (km) for (a) density, (b) temperature, (c) salinity, (d) chlorophyll *a*, and (e) zooplankton.

migration signal is observed as an increase in the overall biomass levels in the upper 120 m during the night, rather than as a re-distribution of zooplankton biomass within the upper 120 m of the water column.

The vertical distributions of the modal amplitudes of the two EOFs of the night zooplankton biomass data are similar to those observed for the total data set and explain approximately the same proportions of the remaining variability (Fig. 13). There are two primary reasons for the similarity between the night zooplankton biomass EOFs and the total zooplankton EOFs: (i) the average variance of the night data is almost six times greater than the variance of the day zooplankton biomass data, hence this variability is more influential in the total zooplankton biomass EOF calculations; and (ii) there are more samples collected at night than during the day (order 2700 versus 2100 profiles). In contrast, the EOFs for the day zooplankton biomass data are dissimilar to those for the night, with

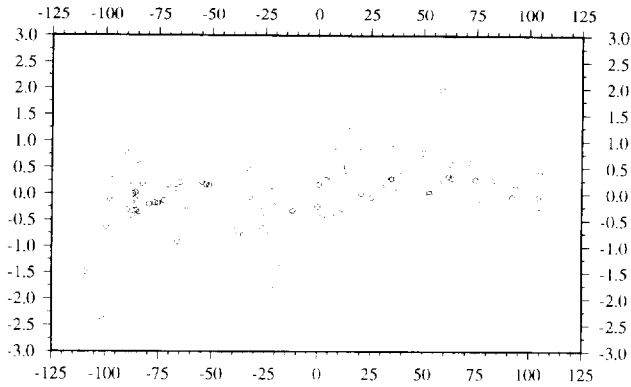


Fig. 10. The distribution of the first principal component of chlorophyll *a* as a function of along-stream distance (km).

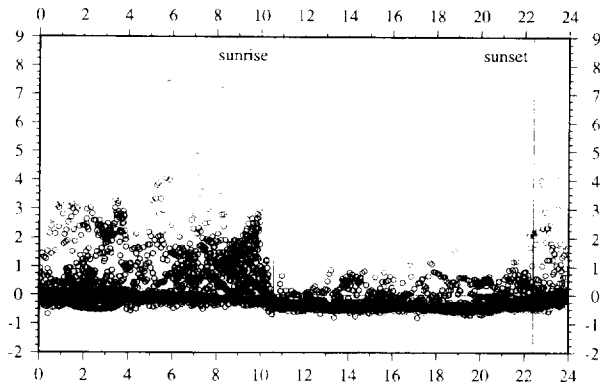


Fig. 11. The distribution of the first principal component of zooplankton as a function of time of day. The average sunrise and sunset for the experiment are plotted as vertical lines.

the second mode showing no sign change with depth (not shown). Furthermore, the variance is apportioned differently among the various modes for day and night samples, although the total variance explained by the sum of the first two modes is similar (Fig. 13(a)). No other significant temporal dependence is observed in the zooplankton PC distributions. The first (Fig. 14) and second (Fig. 15) zooplankton PCs for both day and night demonstrate spatial dependence about the meander, with elevated biomass indicated by the first and second components in the region north of the current axis and east of the crest. The spatial patterns observed for the second PC in the night data are particularly interesting, since the magnitude may vary with the vertical distribution of biomass in the water column. Negative values for the second PC suggest that biomass is greater than the mean in the depth range 20–45 m, and less than the mean below 45 m. The contrast between positive first PCs and negative second PCs in the region north of the axis and west of the crest, where biomass is enhanced, may indicate that some of the variability associated with the enhancement occurred primarily above 45 m.

The spatial distribution of the first and second PCs for both the day and night zooplankton data are plotted in Fig. 14 (day) and Fig. 15 (night) in the local curvilinear

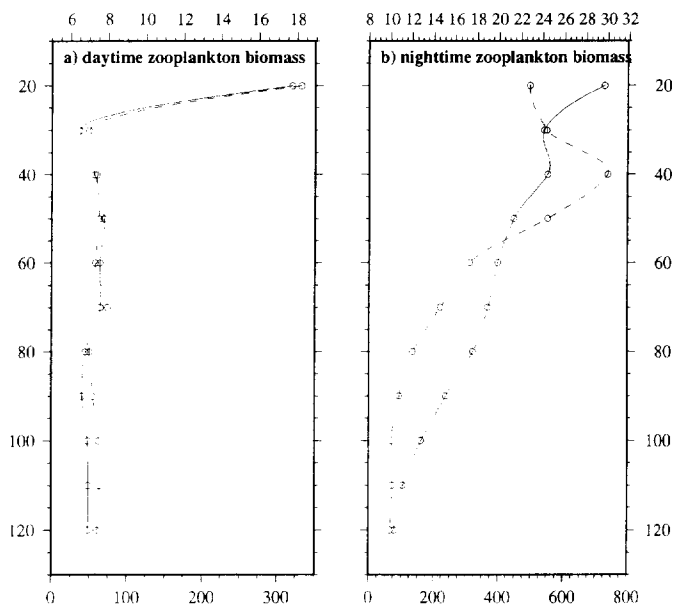


Fig. 12. Like Fig. 1, but for (a) daytime zooplankton and (b) nighttime zooplankton biomass ( $\text{mg}/\text{m}^3$ ).

coordinate system. All four plots demonstrate spatial dependence about the meander, with low amplitude variability in the Gulf Stream core and further south an elevated biomass, indicated by positive first and second components, in the region north of the current axis and east of the crest. The large positive variability in the night data occurs along a 50 km-wide band north of the north wall and a 100 km-long band east of the meander apex. A similar positive variability is observed in the day data in the same region, however the magnitude and spatial extent of this positive variability is somewhat reduced relative to the pattern observed in the night data. These spatial scales of 50–100 km are consistent with those of the physical fields and chlorophyll *a* (Figs 7 and 8; Hitchcock *et al.*, 1993).

### 3.5. Robustness of the results

As discussed in Section 2.3, the elegance of PCA is compromised when the optimal statistical modes, in a variance-explaining sense, are used for dynamical inference. Therefore, the robustness of the results must be verified. To this end, the spline smoothness parameter that determines the subjective mean + variability decomposition and the input data are varied. The input data are also varied to look for subdomain instability and domain dependent modes, by changing both profiles used and the depth range analyzed. For example, salinity and temperature data from the R.V. *Endeavor* between 10 and 230 m are analyzed separately ( $\approx$  half the data set). The EOF modes for this case are practically identical and, as expected, the PC fields from the smaller data set are less detailed. Nevertheless, they exhibit similar primary patterns. Thus, the shapes of the modes presented here are not influenced by sampling strategy.

The spline (inverse) smoothness parameter is varied by three orders of magnitude between

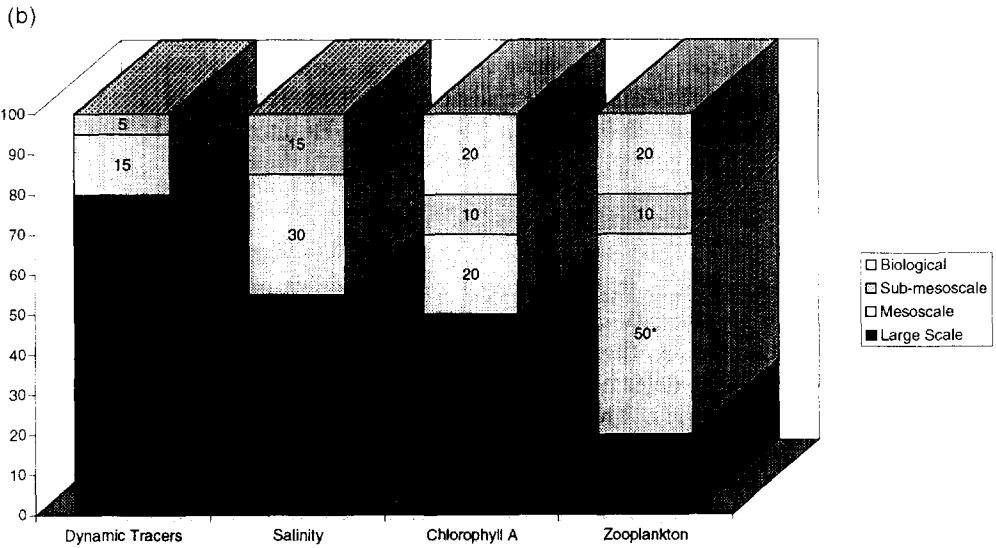
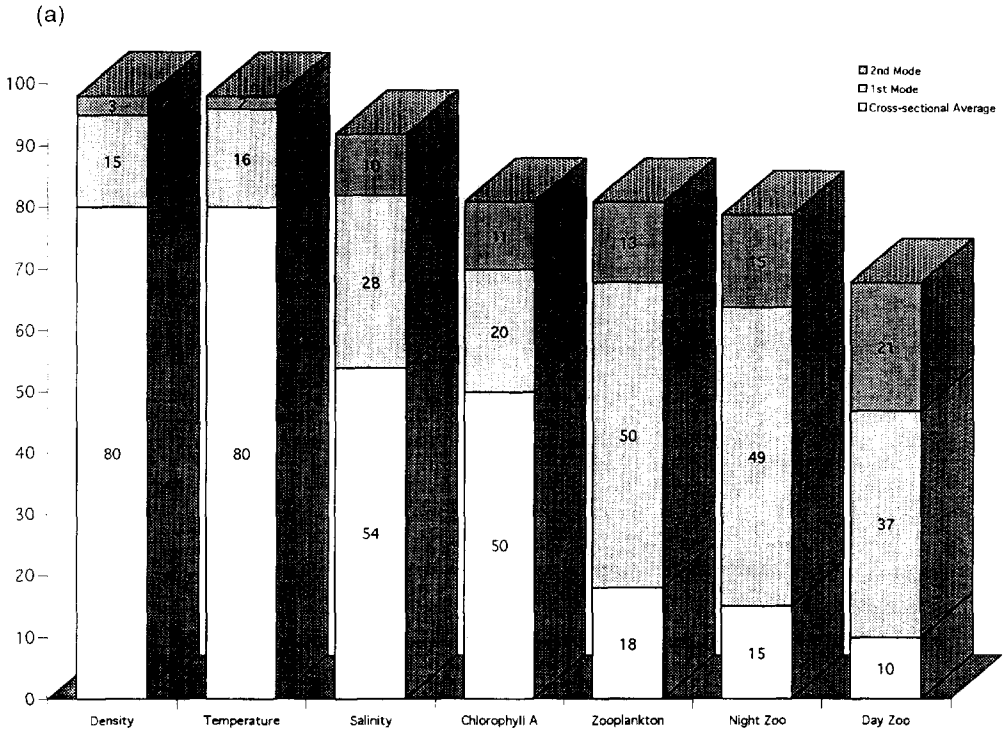


Fig. 13. (a) Data variance explained by decomposition for the physical and biological variables. (b) A summary of data variance explained by different components. \*Includes a major contribution from diel migration.

0.1 (smoothest) and 10.0 (see Inoue (1986)) to examine the sensitivity of our results to this crucial analysis parameter. There is only one noticeable difference in the modal shapes, with the salinity mode being smoother. Also, the detrended variance explained by the first two modes for each variable varies by less than 5% over this range of the smoothness parameter. The principal component pattern also changes in a predictable manner (not shown), with the cross-sectional trends becoming smoother. Consequently the cross-sectional trends capture less of the cross-stream variability with an increase in the cross-stream structure of the corresponding PCs when the inverse smoothness parameter is reduced from 10.0 to 0.1. Nine additional analyses also yielded the same conclusions as those described here.

The salinity and density EOFs are calculated from the same set of profiles, while the temperature EOFs are calculated from a larger data set that is augmented by XBTs. If the EOF shape is strongly influenced by sampling, we would expect to see a tighter correspondence between the EOFs of salinity and density. However, there is a tighter correspondence between temperature and density, indicating that sampling biases are probably minimal for the PCA. Based on this result, and those of the nine complete analyses which incorporated thousands (not all independent) of high quality data points, we conclude that the results presented here are robust.

#### 4. DISCUSSION

The detailed PCA of the bio-physical variability in the meander-based coordinate system provides a means of relating the observed variability in each of the physical and biological fields to the dominant physical mechanisms which influence the dynamics of the meander. This has also furthered our collective effort to determine how the physical processes influence the distribution of plankton about the meander crest (see Hitchcock *et al.*, 1993; Ashjian *et al.*, 1994; Olson *et al.*, 1994). A summary of the total variance explained by the mean cross-sections and the first two statistical modes is shown for each variable in Fig. 13. The PCA indicates that within the range of depths which contains the largest variance of the biophysical fields, a large proportion of the variance in both the physical fields and chlorophyll *a* is explained by the mean cross-section (50–80%). This variance is obviously related to the strong gradients of the persistent Gulf Stream front and can be associated with the large-scale variability. The dominant process which maintains these gradients is the shoaling of the nutricline/pycnocline into the euphotic zone along the cyclonic edge of the Stream.

The variance observed in the first EOFs of the physical and chlorophyll *a* data set, on the order of 20–30% of the total data variance, is associated with mesoscale dynamics of the meander. The spatial scales evident in the PC maps are the same order, 50–100 km, as those scales calculated from three-dimensional (longitude, latitude, time) correlation functions and are the same order as the Rossby radius of deformation. It has been well known since the MODE and POLYMODE experiment that these latter two scales are associated with mesoscale dynamics (Robinson, 1983). Given that these are the dominant scales in the first PC maps, our first mode represents mesoscale variability. The mesoscale dynamics include processes which influence distributions along the front such as meander-induced upwelling and detrainment on the western flank, downwelling and entrainment on the eastern flank, and ring-Stream interactions. Those motions are associated with a weakening of the stream front or frontolysis to the west of the crest and increasing gradients or frontogenesis going into the cyclonic portion of the meander.

The dynamics which induce upwelling and downwelling motions are central to determining how physical processes influence plankton distributions in the BIOSYNOP Study. There are many studies on the vertical motions in geophysical fronts. Newton (1978) drew on analogies between the atmospheric jet stream and the Gulf Stream and hypothesized that the observed three-dimensional motions in a meandering current can be explained with a gradient wind balance, as proposed for atmospheric jets by Bjerknes and Holmboe (1944). Similar arguments can also be invoked on the conservation of potential vorticity to explain the observed frontal patterns and their associated convergent and divergent regions in an unstable meander (e.g. Hoskins and Bretherton, 1971; Hoskins *et al.*, 1978; Pollard and Regier, 1992; Hitchcock *et al.*, 1993). The observed meander-induced dynamics appear to be consistent with existing theories.

Our analysis suggests that variability due to the ring stream interaction is on the same order of magnitude as that associated with upwelling and downwelling in the meander. The ring stream interaction is clearly seen in the satellite imagery (see Discussion and color plate 1 of Hitchcock *et al.*, 1993; Lohrenz *et al.*, 1993), in observed (Fig. 16(a)) and simulated float trajectories (Fig. 16(b)), and in similar numerical simulations by the Harvard Gulfcast (Scott Glenn, Rutgers University, personal communication, October 1988). The simulated float trajectories were calculated in real-time at sea with the Harvard Open Ocean Quasi-geostrophic model in the Gulfcasting configuration described in Robinson *et al.* (1988) with 12 layers, 15 km resolution, feature-models for the stream and rings, and a standard fourth-order Runge–Kutta integration scheme (e.g. Riser, 1982) for displacing numerical floats. The numerical and quasi-Lagrangian observations both indicate a significant water exchange during the interaction consistent with the satellite imagery. Hummon (1995) estimated that 5 Sv of flow in the upper 225 m is advected around the ring during this interaction. The ring stream interaction enhanced the positive PC values for temperature and salinity (Fig. 7) by advecting the apex of the meander crest, and its associated properties, clockwise around the western side of the ring. On the other side of the ring, relatively cool and fresh Slope Water is being advected into the region east of the meander apex; this advection enhanced the negative PC values for temperature and salinity.

The meander-induced upwelling along the western side of the crest also appears to have influenced the distribution of phytoplankton biomass. The localized region of relatively cool waters present west of the meander apex is interpreted as evidence of upwelling and detrainment of cooler, potentially nutrient-rich, waters from the pycnocline. This distribution agrees with that predicted by theory, as discussed above, and the results of a quasi-geostrophic model of meander dynamics which predicts nutrient and plankton biomass fields (Flierl and Davis, 1993). The model results also suggest that as the curvature of a meander decreases, and the wavelength increases, any enhancement of phytoplankton biomass would be displaced further downstream. In a prior study of pigment distribution about the meander crest we hypothesized that the upwelling resulted in enhanced pigment concentrations as the nutrient-rich waters of the pycnocline are upwelled along the western side of the feature (Hitchcock *et al.*, 1993). Diapycnal processes are also potentially important in maintaining the flux of “new” nutrients to the euphotic zone (Pelegri and Csanady, 1994). The sharp pigment maximum in the front consistently tracked the 24.4–25.7  $\sigma_{\theta}$  surfaces (Hitchcock *et al.*, 1993), which are shallower than density surfaces that correspond to the highest nutrient concentrations (Pelegri and Csanady, 1991). Detectable nitrate concentrations are found throughout the upper pycnocline (Lohrenz *et al.*, 1993). However, the variability inherent in the successive surveys about the meander did not

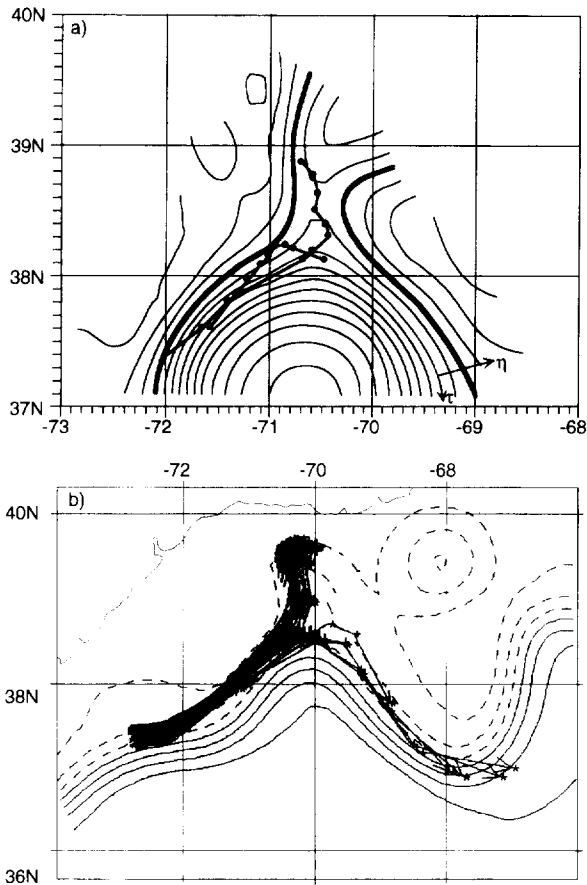


Fig. 16. (a) The trajectories of two RAFOS floats superimposed on an objective analysis map of the depth of the 12 degree isotherm for year day 269. The bold contour corresponds to the nominal location of the North Wall,  $Z_{12} = 300$  m; the dashed contour corresponds to  $\tau$  coordinate axis,  $Z_{12} = 400$  m and  $\eta = 0$ ; and the contour interval is 50 m. Also shown are the two positive axes of the curvilinear coordinate system. (b) 81 simulated trajectories superimposed on a streamfunction map from a real-time Lagrangian prediction at sea performed by Mariano. There is only a qualitative agreement between the actual and the predicted trajectories.

provide a consistent mesoscale pattern of chlorophyll *a* distribution. Hence, it was not possible in our prior study to separate the effects of upwelling from that of the ring stream interaction.

The PCA, in contrast, is able to partition the variability in the pigment distribution and identify the regions of enhanced pigment biomass. There is no evidence of enhanced biomass on the western side of the crest associated with upwelling. A localized maximum in phytoplankton pigment biomass is, however, located east of meander crest and centered near the north wall. The location of the maximum in the Stream-based coordinate system coincided with the region of entrained Slope Water and the zooplankton biomass maximum. Models from simple Lagrangian calculations to eddy resolving primitive equation simulations of the Gulf Stream (Olson *et al.*, 1994) suggest that the pattern

observed in the phytoplankton can arise from a simple meandering stream. The nutrient addition to the euphotic zone does occur just prior to the crest. The time it takes the phytoplankton to respond, however, moves the resultant increase in biomass downstream. In numerical simulations with a linearized nutrient, phytoplankton, zooplankton, and detritus model (Olson *et al.*, 1994) the maximum in phytoplankton occurs along the northern edge of the stream from the crest down into the trough. This pattern is quasi-stationary over timescales of weeks. It is interesting that the zooplankton fields in the models are somewhat similar but of much weaker magnitude than those in the observations. This is because the timescale required to produce zooplankton is very long compared to the meander/phytoplankton response time. We conjecture that the observed zooplankton distribution is due to purely cross-stream advection or involves an interaction between zooplankton behavior and near surface convergence (Olson and Backus, 1985).

Differences in the magnitude of variability between the western and eastern flanks of the meander crest are enhanced by the asymmetrical distribution of horizontal divergence. Yoshimori (1994) showed, for a simple  $1\frac{1}{2}$  layer thin jet model, that this asymmetry, with larger upwelling velocities than downwelling velocities, increases with increasing Rossby number. The upwelling signal in the first temperature PC map (Fig. 7(b)) is stronger than the downwelling signal, supporting the theoretical results. Consequently, in a Lagrangian framework following the phytoplankton, there is a net vertical input of nutrients that can be utilized for enhanced reproduction as the population is advected downstream.

Future modeling of the interactions between phytoplankton and zooplankton in strongly baroclinic systems such as the Gulf Stream should take into account that each population is associated with different physical surfaces. The distribution of phytoplankton is mostly tied to isopycnal surfaces, while the distribution of zooplankton may be a function of both light intensity, which is mostly a function of depth (or equivalently, pressure), and environmental characteristics such as temperature, salinity and hence density (see Wishner and Allison, 1986; Ashjian and Wishner, 1993b). Thus, for a given isopycnal layer that intersects many different pressure surfaces, there will be localized regions and times of strong or weak interactions leading to either elevated or depressed zooplankton and phytoplankton biomass. Through advection and turbulent mixing, it is easy to envision that the plankton biomass distribution must be patchy, but detailed numerical investigation of this patchiness is complicated and is in its infancy. Our analysis will be an important benchmark for these studies.

The principal component analysis accounts for approximately 70–80% of the overall variability in the distribution of zooplankton biomass. Although the cross-stream gradient in zooplankton biomass is a dramatic signature of the Gulf Stream front (e.g. Allison and Wishner, 1986), surprisingly this feature (represented by the cross-stream mean) accounts for less than 20% of the observed variability in the zooplankton biomass distribution. The dominant sources of variation in the biomass distribution are the factors contributing to the distribution of the first PC. Our initial analysis, utilizing all zooplankton data, demonstrates that the distribution of the first PC is sensitive to changes in the magnitude of zooplankton biomass that occur as a consequence of diel vertical migration. Once the diel signal is removed by considering the day and night data separately, the cross-stream gradient in zooplankton biomass accounted for even less of the total observed variability (10.3% and 14.7% for day and night, respectively) than in the total data set. The remaining 60% of the variability is divided between the first two principal components. Given the extremely patchy distribution of zooplankton biomass, and the variability in zooplankton community

compositions and biomass levels in distinct water masses, it is striking that the analysis is able to account for a large proportion of the total variability (79 and 68% for night and day, respectively, Fig. 13(a)).

The separation of the day and night data effectively removed the biological signal of diel vertical migration and provided a means for considering the spatial patterns. For zooplankton, the spatial distributions should be influenced primarily by physical processes, such as advection or concentration and dilution, or by the interaction of behavior (swimming) with the flow field, rather than by reproduction, since the timescales for such a response by the zooplankton in the sampled size class are much longer than the advective timescale of a meander (e.g. Mackas and Boyd, 1979; Okubo, 1980; Mackas *et al.*, 1985; Flierl and Davis, 1993; Olson *et al.*, 1994).

The spatial distributions of the first and second principal components (Figs 8(b), 14 and 15) suggest that zooplankton biomass is influenced by the cross-frontal advection characteristic of meanders, especially to the north of the Gulf Stream axis. For all data (total, day and night) the region to the east of the crest has enhanced biomass levels, while reduced biomass is observed west of the crest, relative to the cross-stream mean. The observed patterns may be explained by the hypothesized advection and exchange of water types across a meander. Hence regions to the west of the crest, especially near the axis, may contain zooplankton communities characteristic of the Gulf Stream or Sargasso Sea, with low levels of biomass. In contrast, regions to the east of the crest may be characterized by zooplankton communities characteristic of the Slope Water with higher levels of biomass. This conclusion is born out in the similarity between the salinity (Fig. 7(c)) and zooplankton patterns (Fig. 8(b)) where low salinity and high zooplankton both correspond to slope/shelf contributions.

The spatial distributions of integrated zooplankton biomass (20–100 m) during both day and night are similar to the distributions of the first PCs (Ashjian *et al.*, 1994). This similarity is not surprising, given the vertical distribution of the modal amplitudes of the first EOFs for both day and night data. The spatial variability represented by the first PC reflects changes in the magnitude of zooplankton biomass at most depths in the upper 120 m.

The hypothesized advection of various water types and their associated zooplankton communities about the meander is further supported by the distribution of indicator copepod species (Ashjian, 1993). To some extent, copepod species may be considered as tracers of water types. Slope Water copepod species are found in relatively high abundance north and east of the meander crest, coincident with the region where the PCA indicated elevated biomass levels. In contrast, relatively high abundances of Gulf Stream species are found north and west of the crest apex. Although the observations of the copepod species are obtained at isolated stations across the meander, and at far fewer locations than the zooplankton biomass measurements, the coherence of the observations supports the conclusion that advection strongly influenced the distribution and variability of the zooplankton community.

Unlike the physical variables, the distribution of zooplankton biomass did not exhibit a spatial pattern which could be identified with the ring stream interaction. The zooplankton biomass distribution was sampled from the R.V. *Cape Hatteras*, and slightly later in time than the other variables on the R.V. *Endeavor*. An examination of the cruise track from the *Cape Hatteras* indicates that the sampling for zooplankton biomass distributions did not cross the region of the strongest ring-stream interaction.

The variance explained by the physical and biological processes rounded to the nearest

5% (rationalized next) is given in Fig. 13(b). Note that the difference between the zooplankton night and total zooplankton variance decomposition (Fig. 13(a)) is a few per cent. Also, the difference in large-scale variability between salinity and chlorophyll *a*, both passive tracers, is 5%. Other full analyses, described in Section 3.5, yielded an error of 5% for each term in the variance decomposition. Thus, the error in the variance decomposition terms are on the order of 5%.

The variance structure of the dynamical tracers, density and temperature, is explained by 80% large-scale variability and 15% mesoscale variability, leaving 5% for sub-mesoscale and measurement variance. The measurement noise is negligible compared to the sub-grid scale noise (see Mariano and Brown, 1992). For this experiment, sub-grid scales are scales less than 20 km, the nominal station spacing. The mesoscale is on the order of 50–100 km based on the dominant patterns in the spatial PC distributions and the correlation analysis performed by Hitchcock *et al.* (1993), so the sub-grid scale noise can be associated with sub-mesoscale processes. The variance structure of salinity, a passive tracer, is 55% for large-scale variability and 30% for mesoscale variability, leaving 15% for sub-mesoscale processes.

There may also be leakage between scales in this analysis, and some of the 5% variability for temperature/density and 15% variability for salinity may be associated with mesoscale variability not represented by the first mode. There are 50–100 km patterns in the second PC maps that may be a signature of this leakage or may indicate that the energetics of sub-mesoscale processes are coupled to the energetics of mesoscale processes. It should also be noted that some of the larger patterns in the second PC maps are very low amplitude and are in the noise of our analysis. It is difficult to use the EOFs themselves for determining the scales since the shape of the second mode is mostly determined by the shape of the first mode and the orthogonality constraint in the PCA. We will associate the second statistical modes with sub-mesoscale variability. On the average, the second modes of the physical variables account for 10% of the variability.

The variance structure of chlorophyll *a* is 50% for large-scale variability and 20% for mesoscale variability. Assuming a value of 10% for sub-mesoscale variability produced by purely physical processes, based on the average for the physical variables, leaves 20% of the variability to be explained by biological processes. These processes include such factors as microzooplankton grazing and the spatial gradients in herbivores associated with physical or biological processes.

Only 20% of the zooplankton variance is due to large-scale variability, while 50% of the variability is due to mesoscale processes, which are enhanced by diel migration. In the Gulf Stream, mesoscale phenomena have timescales on the order of weeks, while the timescale of diel migration is much faster (1 day). Thus, diel migration effects are integrated many times during a typical mesoscale event, enhancing the effects of mesoscale stirring. If 10% of the remaining variability is attributed to sub-mesoscale physical processes, the remaining 20% may be assumed to be biological processes other than diel migration, such as predation, competition, mortality, reproduction, or feeding behavior.

In summary, a comparison of the spatial distributions of the first principal components for all the variables considered in this analysis reveals similar patterns existed across the meander. For all variables, the region to the north of the current axis and east of the crest is characterized by properties characteristic of Slope Water (colder, fresher water with high concentrations of chlorophyll and zooplankton biomass). The region to the west of the crest, in contrast, is characterized by diminished levels of both chlorophyll and zooplankton

biomass. These zooplankton patterns are considered to arise primarily as a result of cross-stream advection rather than as a production response (Flierl and Davis, 1993). The advection hypothesis is supported by the spatial maps of the first PC where the primary "negative" pattern in the passive tracer salinity (Fig. 7(c)) corresponds pretty well with the primary "positive" pattern in zooplankton biomass (Fig. 8(b)), especially for the night PC distribution (Fig. 15). However, given the potentially short response of phytoplankton to enhanced nutrients, both advection and upwelling may have a significant impact on pigment distributions. Through coordinated sampling and a detailed quantitative analysis, the PCA has identified key factors which likely regulate the temporal/spatial variability of biophysical fields about a Gulf Stream meander crest. The results of this study should be useful as a benchmark for future modeling studies which seek to couple physical processes with the distributions of plankton about Gulf Stream meanders.

*Acknowledgements*—The analysis presented here was supported by the Office of Naval Research Random Fields in Oceanography ARI under Grant N00014-91-J-1120 to A. J. Mariano. The BIOSYNOP program was funded by the Office of Naval Research under grants N00014-89-J1536 (Olson), N00014-88-F-0097 (Smith), and N00014-91J-1610 (Hitchcock). The Anatomy of a Meander experiment was funded under grants NSF OCE 87-16924 and ONR N00014-87-K-0235 (Rossby). We would like to thank E. F. Carter, C. N. Flagg, J. Hummon, J. L. Lillibridge III, and G. Samuels for their support in data acquisition and processing. This study was presented at the 1994 Summer Study Program in Geophysical Fluid Dynamics, and final preparation of the manuscript was supported by NSF OCE#93-14484 to W.H.O.I. Comments by two anonymous reviewers and the editor, M. P. Bacon, greatly improved the manuscript.

## REFERENCES

- Allison S. K. and K. F. Wishner (1986) Spatial and temporal patterns of zooplankton biomass across the Gulf Stream. *Marine Ecology Progress Series*, **31**, 233–244.
- Ashjian C. J. (1993) Trends in copepod species abundances across and along a Gulf Stream meander: Evidence for entrainment and detrainment of fluid parcels from the Gulf Stream. *Deep-Sea Research I*, **40**, 461–482.
- Ashjian C. J. and K. F. Wishner (1993a) Temporal and spatial changes in body size and reproductive state of *Nannocalanus minor* (Copepoda) females across and along the Gulf Stream. *Journal of Plankton Research*, **15**, 67–98.
- Ashjian C. J. and K. F. Wishner (1993b) Temporal consistency of copepod species groups in the Gulf Stream. *Deep-Sea Research I*, **40**, 483–516.
- Ashjian C. J., S. L. Smith, C. N. Flagg, A. J. Mariano, W. J. Behrens and P. V. Z. Lane (1994) The influence of Gulf Stream Meander on the distribution of zooplankton biomass in the Slope Water, the Gulf Stream, and the Sargasso Sea. *Deep-Sea Research I*, **41**, 23–50.
- Bjerknes J. and J. Holmboe (1944) On the theory of cyclones. *Journal of Meteorology*, **1**, 1–22.
- Blasco D. (1971) Composition and distribution of phytoplankton in the upwelling region of the Peruvian Coast. (Composicin y distribucion del fitoplancton en la region de l afloramiento de las costas peruanas.). *Investigación Pesquera*, **35**, 61–112.
- Bower A. S. and T. Rossby (1989) Evidence of cross-frontal exchange processes in the Gulf Stream based on isopycnal RAFOS float data. *Journal of Physical Oceanography*, **19**, 1177–1190.
- Chavez F. P., R. T. Barber, P. M. Kosro, A. Huyer, S. R. Ramp, T. P. Stanton and B. Rojas de Mendiola (1991) Horizontal transport and the distribution of nutrients in the Coastal Transition Zone off Northern California: Effects on primary production, phytoplankton biomass, and species composition. *Journal of Geophysical Research*, **96**, 14,809–14,832.
- Chin and Mariano (in press) Space–time interpolation of Oceanic Fronts. *IEEE Journal of Geoscience and Remote Sensing*.
- Cornillon P. and D. R. Watts (1987) Satellite thermal infrared and inverted echo sounder determinations of the Gulf Stream Northern Edge. *Journal of Atmospheric and Oceanic Technology*, **4**, 713–723.
- Denman K. and T. Platt (1978) Time series analysis in marine ecosystem. In: *Time series and ecological processes*, H. H. Shugart, Jr, editor. Siam Institute for Mathematics and Society. Philadelphia, PA, pp. 227–242.

- Flierl G. R. and C. S. Davis (1993) Biological effects of Gulf Stream meandering. *Journal of Marine Research*, **51**, 529–560.
- Garfield N. and D. L. Evans (1987) Shelf water entrainment by Gulf Stream Warm Core Rings. *Journal of Geophysical Research*, **92**, 13,003–13,012.
- García-Moliner G., D. M. Mason, C. H. Greene, A. Lobo, B. Li, J. Wu and G. A. Bradshaw (1993) Description and analysis of spatial patterns. In: *Lecture notes in mathematics*, S. A. Levin, T. M. Powell and J. H. Steele, editors, Springer-Verlag, Heidelberg, pp. 70–89.
- Garvine R. W. (1988) Flow field properties of long, propagating frontal waves. *Journal of Physical Oceanography*, **18**, 788–792.
- Grice G. D. and A. D. Hart (1962) The abundances, seasonal occurrence, and distribution of epizooplankton between New York and Bermuda. *Ecological Monographs*, **32**, 287–309.
- Halkin D. and T. Rossby (1985) The structure and transport of the Gulf Stream at 73° west. *Journal of Physical Oceanography*, **15**, 1439–1452.
- Hansen D. V. and G. A. Maul (1970) A note on the use of sea surface temperature from observing ocean currents. *Remote Sensing of the Environment*, **1**, 161–164.
- Hitchcock G. L., A. J. Mariano and T. Rossby (1993) Mesoscale pigment fields in the Gulf Stream: Observations in a meander crest and trough. *Journal of Geophysical Research*, **98**, 8425–8445.
- Hoskins B. J. and F. P. Bretherton (1971) Atmospheric frontogenesis models: Mathematical formulation and solution. *Journal of Atmospheric Science*, **29**, 11–37.
- Hoskins B. J., I. Draghici and H. C. Davies (1978) A new look at the  $\omega$ -equation. *Quarterly Journal of the Royal Meteorological Society*, **104**, 31–38.
- Hummon J. (1995) Gulf Stream warm Core Ring Interaction, Ph.D. Dissertation, Graduate School of Oceanography, URI, 1995, 181 pp.
- Hummon J., T. Rossby, E. Carter, J. Lillibridge, M. Liu, K. Schultz Tokos, S. Anderson-Fontanta and A. Mariano (1991) The anatomy of Gulf Stream Meanders, Volume I: Technical description and fall cruise data. GSO URI Tech. Report 91–4. 254 pp.
- Hurlburt E. W. (1964) Succession and diversity in the plankton flora of the western North Atlantic. *Bulletin of Marine Science*, **14**, 33–44.
- Inoue H. (1986) A least-square smooth fitting for irregularly spaced data: finite-element approach using the cubic B-spline. *Geophysics*, **51**, 2051–2066.
- Jassby A. D. and T. M. Powell (1990) Detecting changes in ecological time series. *Ecology*, **71**, 2044–2054.
- Lillibridge J. L., G. L. Hitchcock, T. Rossby, E. J. Lessard, M. Mork and L. Golmen (1990) Entrainment and mixing of shelf/slope waters in the near-surface Gulf Stream. *Journal of Geophysical Research*, **95**, 13,065–13,087.
- Lohrenz S. E., D. A. Phinney, C. S. Yentsch and D. B. Olson (1993) Pigment and primary production distributions in a Gulf Stream meander. *Journal of Geophysical Research*, **98**, 14,545–14,560.
- Mackas D. L. and C. M. Boyd (1979) Spectral analysis of zooplankton spatial heterogeneity. *Science*, **204**, 62–64.
- Mackas D. L., K. L. Denman and M. R. Abbott (1985) Plankton patchiness: Biology in the physical vernacular. *Bulletin of Marine Science*, **37**, 652–674.
- Mackas D. L., L. Washburn and S. L. Smith (1991) Zooplankton community pattern associated with a California Current Cold Filament. *Journal of Geophysical Research*, **96**, 14,781–14,798.
- Mariano A. J. (1990) Contour analysis: A new approach for melding geophysical fields. *Journal of Atmospheric and Oceanic Technology*, **7**, 285–295.
- Mariano A. J. and O. B. Brown (1992) Efficient objective of dynamically heterogeneous and nonstationary fields via the parameter matrix. *Deep Sea Research*, **39**, 1255–1271.
- Mariano A. J. and G. L. Hitchcock (1993) Bio-physical variability in the upper 200 m of a Gulf Stream meander crest. Abstracts of the Third Scientific Meeting of The Oceanography Society, 13–16 April, Seattle, WA.
- Newton C. W. (1978) Fronts and wave disturbances in Gulf Stream and atmospheric Jet Stream. *Journal of Geophysical Research*, **83**, 4697–4706.
- Okubo A. (1980) *Diffusion and ecological problems: Mathematical models*, Springer-Verlag, New York, 254 pp.
- Olson D. B. (1986) Lateral exchange within Gulf Stream ring surface layers. *Deep-Sea Research*, **33**, 1691–1704.
- Olson D. B. (1991) Rings in the ocean. *Annual Reviews of Earth and Planetary Science*, **19**, 283–311.
- Olson D. B. and R. H. Backus (1985) The concentrating of organisms at fronts: a cold-water fish and warm-core Gulf Stream ring. *Journal of Marine Research*, **43**, 113–137.
- Olson D. B., G. Hitchcock, A. J. Mariano, C. Ashjian, G. Peng, R. W. Nero and G. Podestá (1994) Life on the edge: Marine life and fronts. *Oceanography*, **7**, 52–60.

- Pelegrí J. L. and G. T. Csanady (1991) Nutrient transport and mixing in the Gulf Stream. *Journal of Geophysical Research*, **96**(C2), 2577–2583.
- Pelegrí J. L. and G. T. Csanady (1994) Diapycnal mixing in western boundary currents. *Journal of Geophysical Research*, **99**(C9), 18,275–18,304.
- Pollard R. T. and L. A. Regier (1992) Vorticity and vertical circulation at an ocean front. *Journal of Physical Oceanography*, **22**, 609–625.
- Preisendorfer R. W. (1988) *Principal component analysis in meteorology and oceanography*. Elsevier, NY, 425 pp.
- Richman M. B. (1986) Rotation of principal components. *Journal of Climatology*, **6**, 293–335.
- Riser S. C. (1982) On the Quasi-Lagrangian nature of SOFAR floats. *Deep-Sea Research*, **12A**, 1587–1602.
- Robinson A. R. (1983) *Eddies in marine science*. Springer-Verlag, New York, 609 pp.
- Robinson A. R., M. A. Spall and N. Pinardi (1988) Gulf Stream simulations and the dynamics of ring and meander processes. *Journal of Physical Oceanography*, **18**, 1811–1853.
- Strub P. T., P. M. Kosro and A. Huyer (1991) The nature of the cold filaments in the California Current system. *Journal of Geophysical Research*, **96**, 14,743–14,768.
- Wishner K. F. and S. K. Allison (1986) The distribution and abundance of copepods in relation to the physical structure of the Gulf Stream. *Deep-Sea Research*, **23**, 705–731.
- Yoshimori A. (1994) Horizontal divergence caused by meanders of a thin jet. *Journal of Physical Oceanography*, **24**, 345–352.